

# MULTILEVEL OPTIMAL TRANSPORT: A FAST APPROXIMATION OF WASSERSTEIN-1 DISTANCES\*

JIALIN LIU<sup>†</sup>, WOTAO YIN<sup>†</sup>, WUCHEN LI<sup>†</sup>, AND YAT TIN CHOW<sup>‡</sup>

**Abstract.** We propose a fast algorithm for the calculation of the Wasserstein-1 distance, which is a particular type of optimal transport distance with homogeneous of degree one transport cost. Our algorithm is built on multilevel primal-dual algorithms. Several numerical examples and a complexity analysis are provided to demonstrate its computational speed. On some commonly used image examples of size  $512 \times 512$ , the proposed algorithm gives solutions within  $0.2 \sim 1.5$  seconds on a single CPU, which is much faster than the state-of-the-art algorithms.

**Key words.** Multilevel algorithms; Optimal transport; Wasserstein-1 distance; Primal-dual algorithm.

**AMS subject classifications.** 49M25; 49M30; 90C90

**1. Introduction.** Optimal transport (OT) plays crucial roles in many areas, including fluid dynamics [54], image processing [45, 46], machine learning [1, 25] and control [16, 17]. It is a well-posed distance between two probability distributions over a given domain. The distance is often named Earth Mover’s distance (EMD) or the Wasserstein distance. Plenty of theories on OT have been introduced [5, 6, 26, 38, 54, 11]. Despite the theoretical development, computing the distance is still challenging since the OT problems usually do not have closed-form solutions. Fast numerical algorithms are essential for the related applications.

Recently, a particular class of OT, named the Wasserstein-1 distance, has been widely used in machine learning problems [1, 28, 43]. It gains rising interest in the computational mathematics community [49, 50, 30, 34, 4] [53, Section 3.1]. The Wasserstein-1 distance is named as its transport cost is homogeneous of degree one. In this paper, we focus on numerically computing Wasserstein-1 distances.

In the literature, many numerical schemes have been proposed for the OT problem. [32, 45, 35, 42, 41, 37, 2, 4] modeled the OT problem as linear programming (LP) with specific structures. They utilized these structures to develop efficient solvers. [39, 44, 7, 29, 34, 33, 47] modeled OT as a nonsmooth convex optimization problem and introduced iterative algorithms to solve it. [19, 8, 52, 23, 14, 24, 20, 10] studied the OT problems with regularizers and proposed efficient algorithms to solve them. In particular, some algorithms have been developed for calculating the Wasserstein-1 distance and its variants. Ling and Okada [35] exploited the structure of the problem to improve the transportation simplex algorithm [32] and proposed Tree-EMD. Pele and Werman [41, 42] proposed and solved EMD with a thresholded ground metric. Bartel and Schön [3] added a regularization term on the original problem and introduced primal-dual algorithms to solve it. Li et al. [34] studied a primal-dual algorithm for calculating Wasserstein-1 distances that is friendly to parallel programming and has an implementation on CUDA. Jacobs et al. [33] introduced the proximal PDHG method, whose number of iterations is independent of the grid size. Bassetti et al.

\*The codes will be released to: <https://github.com/liujl11git/multilevelOT>.

**Funding:** The research is supported by AFOSR MURI FA9550-18-1-0502, ONR N000141712162 and NSF DMS-1720237. The Titan Xp used for this research was donated by the NVIDIA Corporation.

<sup>†</sup>Department of Mathematics, University of California, Los Angeles. (liujl11@math.ucla.edu; wotaoyin@math.ucla.edu; wcli@math.ucla.edu)

<sup>‡</sup>Department of Mathematics, University of California, Riverside. (yattinc@ucr.edu)

[4] studied the connections between the Wasserstein-1 distance and the uncapacitated minimum cost flow problem and applied the network simplex algorithm to solve it.

*Motivations and our contributions.* Although many numerical algorithms [35, 4, 34, 33] have been proposed to calculate the Wasserstein-1 distance, there is still some room to speed them up, especially for large-scale problems, for example, a grid of  $512 \times 512$ . Motivated by the success of multigrid methods [55] for calculating Wasserstein- $p$  ( $p > 1$ ) distance [37, 29, 48, 36], we apply the cascadic multilevel method [12] to calculate Wasserstein-1 distances. We compute the distances on different grid levels and use the solutions on the coarse grids to initialize the calculation of solutions on the finer grids. We use this method to speed up the state-of-the-art algorithms [34, 33], dramatically reducing the computational expense on the finest grids and lessening the total time consumption by  $2 \sim 12$  times. The speedup effect depends on the size of the problem. It is significant for large-scale problems.

The rest of this paper is organized as follows. In Section 2, we briefly review the Wasserstein-1 distance. In Section 3, we demonstrate our multilevel algorithms and provide a complexity analysis in Section 4. In Section 5, we numerically validate the assumptions used in Section 4. Finally, in Section 6, we present several numerical examples.

**2. Problem description.** Given a domain  $\Omega \subset \mathbb{R}^d$ , the EMD, or the Wasserstein distance, is a commonly-used metric to measure the distance between two probability distributions defined on  $\Omega$ :  $\rho^0, \rho^1 : \Omega \rightarrow \mathbb{R}$ . Wasserstein-1 distance is defined by the minimum value of the following minimization problem:

$$(2.1) \quad W_1(\rho^0, \rho^1) = \inf_{\pi \in \Gamma(\rho^0, \rho^1)} \int_{\Omega \times \Omega} \|x - y\|_p d\pi(x, y),$$

where  $\|x - y\|_p, 1 \leq p \leq \infty$ , defines the transport cost between two points  $x, y \in \Omega$ , and  $\Gamma(\rho^0, \rho^1)$  is the set of nonnegative measurements  $\pi$  on  $\Omega \times \Omega$  satisfying

$$\pi(B \times \Omega) = \rho^0(B), \quad \pi(\Omega \times B) = \rho^1(B)$$

for all measurable  $B \subset \Omega$ . The dual problem of (2.1), also named the Kantorovich dual problem, is:

$$(2.2) \quad W_1(\rho^0, \rho^1) = \sup \left\{ \int_{\Omega} \phi^0 d\rho^0 - \int_{\Omega} \phi^1 d\rho^1 \mid \phi^0(x) - \phi^1(y) \leq \|x - y\|_p, \forall x, y \in \Omega. \right\},$$

where  $\phi^0, \phi^1 : \Omega \rightarrow \mathbb{R}$ , are (Kantorovich) dual variables.

In the 1D case ( $d = 1$ ), the Wasserstein Distance has a closed-form solution [54]. With two or higher dimensions ( $d \geq 2$ ), the distance is no longer given in a closed form, and it is obtained via iterative algorithms.

**2.1. Problem settings.** In this paper, we focus on an equivalent and simpler form of (2.2). Since  $\|\cdot\|_p$  is homogeneous of degree one, by [54], there is an equivalent form of (2.2), where  $\phi^0 = \phi^1 = \phi$ . In other words,

$$(2.3) \quad \begin{aligned} & \underset{\phi: \Omega \rightarrow \mathbb{R}}{\text{maximize}} \int_{x \in \Omega} \phi(x)(\rho^0(x) - \rho^1(x)) dx \\ & \text{subject to } \|\nabla \phi(x)\|_q \leq 1, \quad \text{almost everywhere in } \Omega, \end{aligned}$$

where  $1/p + 1/q = 1$  and  $1 \leq q \leq \infty$ . The following minimization problem, which is the dual problem of (2.3), is also considered in this paper:

$$(2.4) \quad \begin{aligned} & \text{minimize}_{m: \Omega \rightarrow \mathfrak{R}^d} \int_{x \in \Omega} \|m(x)\|_p dx \\ & \text{subject to } \operatorname{div}(m(x)) = \rho^0(x) - \rho^1(x), \quad \forall x \in \Omega, \\ & \quad \quad \quad m(x) \cdot n(x) = 0, \quad \forall x \in \partial\Omega, \end{aligned}$$

where “div” denotes the divergence operator  $\operatorname{div}(m(x)) = \sum_{i=1}^d \frac{\partial m_i}{\partial x_i}(x)$  and  $n(x)$  is normal to  $\partial\Omega$ . Here  $m$  is a  $d$  dimensional field satisfying the zero flux boundary condition [5]. The solution of (2.4)  $m^*$  is called “the optimal flux”.

**2.2. Discretization.** We set  $\Omega = [0, 1]^d$ . Let  $\Omega^h$  be a grid on  $\Omega$  with step size  $h > 0$ :

$$\Omega^h = \{0, h, 2h, 3h, \dots, 1\}^d.$$

Let  $N = 1/h$  be the grid size. Any  $x \in \Omega^h$  is a  $d$  dimensional tensor, of which the value of the  $i^{\text{th}}$  component  $x_i$  is chosen from  $\{0, h, 2h, 3h, \dots, 1\}$ . The discretized distributions  $\rho_h^0, \rho_h^1$  are  $(N+1)^d$  tensors, and the discretized flux  $m_h$  is a  $(N+1)^d \times d$  tensor, which represents a map  $\Omega^h \rightarrow \mathfrak{R}^d$ :  $\rho_h^0 = \{\rho^0(x)\}_{x \in \Omega^h}$ ,  $\rho_h^1 = \{\rho^1(x)\}_{x \in \Omega^h}$ , and  $m_h = \{m(x)\}_{x \in \Omega^h}$ . The discretized version of (2.4) can be written as

$$(2.5) \quad \begin{aligned} & \text{minimize}_{m_h: \Omega^h \rightarrow \mathfrak{R}^d} \sum_{x \in \Omega^h} \|m_h(x)\|_p h^d \\ & \text{subject to } \operatorname{div}^h(m_h(x)) = \rho_h^0(x) - \rho_h^1(x), \quad \forall x \in \Omega^h, \end{aligned}$$

where the discrete divergence operator is:

$$\operatorname{div}^h(m_h(x)) = \sum_{i=1}^d D_{h,i} m(x),$$

$$D_{h,i} m(x) = \begin{cases} (m_{h,i}(x_{-i}, x_i))/h, & x_i = 0 \\ (m_{h,i}(x_{-i}, x_i) - m_{h,i}(x_{-i}, x_i - h))/h, & 0 < x_i < 1 \\ (-m_{h,i}(x_{-i}, x_i - h))/h, & x_i > 1. \end{cases}$$

In the definition of  $\operatorname{div}^h$ ,  $m_h(x) \in \mathfrak{R}^d$  means the flow at point  $x$ ,  $m_{h,i}(x) \in \mathfrak{R}$  is the  $i^{\text{th}}$  component of  $m_h(x)$ . The notion “ $-i$ ” refers to all the components excluding  $i$ :  $x_{-i} = \{x_j : j \in \{1, 2, \dots, d\}, j \neq i\}$ .

To simplify our notation, we rewrite the above problem (2.5) as:

$$(2.6) \quad \begin{aligned} & \text{minimize}_{m_h: \Omega^h \rightarrow \mathfrak{R}^d} f(m_h) \\ & \text{subject to } A_h m_h = \rho_h, \end{aligned}$$

where  $f(\cdot)$  denotes a norm of  $m_h$ ,  $A_h$  denotes the divergence operator, which is linear, and  $\rho_h = \rho_h^0 - \rho_h^1$ .

The dual problem of (2.6), which is also the discrete version of (2.3), is:

$$(2.7) \quad \begin{aligned} & \text{minimize}_{\phi_h: \Omega^h \rightarrow \mathfrak{R}} \sum_{x \in \Omega^h} \phi_h(x) \rho_h(x) h^d \\ & \text{subject to } \|A_h^* \phi_h(x)\|_q \leq 1, \quad \forall x \in \Omega^h, \end{aligned}$$

where  $\phi_h : \Omega^h \rightarrow \mathfrak{R}$  is the *Kantorovich potential*:  $\phi_h = \{\phi(x)\}_{x \in \Omega^h}$ . The adjoint operator of  $A_h$ ,  $A_h^*$ , denotes the gradient operator.

In this paper, we solve (2.6) and (2.7) jointly by primal-dual algorithms. Define some norms on  $\Omega^h$ :

$$\begin{aligned} \|m_h\|_2^2 &= \sum_{x \in \Omega^h} \|m(x)\|_2^2, & \|m_h\|_{L^2}^2 &= \sum_{x \in \Omega^h} \|m(x)\|_2^2 h^d, \\ \|\phi_h\|_2^2 &= \sum_{x \in \Omega^h} \phi^2(x), & \|\phi_h\|_{L^2}^2 &= \sum_{x \in \Omega^h} \phi^2(x) h^d, \\ \|\varphi_h\|_2^2 &= \sum_{x \in \Omega^h} \|\varphi(x)\|_2^2, & \|\varphi_h\|_{L^2}^2 &= \sum_{x \in \Omega^h} \|\varphi(x)\|_2^2 h^d. \end{aligned}$$

Define inner products on  $\Omega^h$ :

$$\begin{aligned} \langle \phi_h, \phi'_h \rangle &= \sum_{x \in \Omega^h} \phi_h(x) \phi'_h(x), \\ \langle \phi_h, \phi'_h \rangle_h &= \sum_{x \in \Omega^h} \phi_h(x) \phi'_h(x) h^d. \end{aligned}$$

**3. Algorithm description.** In this section, we review two recent primal-dual algorithms designed for (2.6) and (2.7). We apply a multilevel framework (Section 3.2) to further accelerate these algorithms.

### 3.1. Two recent algorithms for (2.6) and (2.7).

*Algorithm 1* (Li et al. [34]). Problems (2.6) and (2.7) can be jointly solved by the following min-max problem:

$$(3.1) \quad \min_{m_h} \max_{\phi_h} L(m_h, \phi_h), \quad \text{where } L(m_h, \phi_h) = f(m_h) + \langle \phi_h, A_h m_h - \rho_h \rangle_h.$$

Inspired by the Chambolle-Pock Algorithm [15], the authors of [34] proposed the following algorithm to solve (3.1):

$$(3.2) \quad \begin{aligned} m_h^{k+1} &= \arg \min_{m_h} L(m_h, \phi_h^k) + \frac{1}{2\mu} \|m_h - m_h^k\|_{L^2}^2, \\ \bar{m}_h^{k+1} &= 2m_h^{k+1} - m_h^k, \\ \phi_h^{k+1} &= \arg \max_{\phi_h} L(\bar{m}_h^{k+1}, \phi_h) - \frac{1}{2\tau} \|\phi_h - \phi_h^k\|_{L^2}^2. \end{aligned}$$

Parameters  $\mu, \tau > 0$  need to be tuned. If  $\mu\tau \|A_h\|^2 < 1$ , then we have the convergence  $(m_h^k, \phi_h^k) \rightarrow (m_h^*, \phi_h^*)$ , where  $(m_h^*, \phi_h^*)$  is one of the solutions of (3.1). In this paper, we use<sup>1</sup>  $\mu = \tau = 1/(2\|A_h\|)$ . The iteration stops when the following fixed point residual (FPR)  $R^k$  falls below a threshold:

$$(3.3) \quad R_h^k := \frac{1}{\mu} \|m_h^{k+1} - m_h^k\|_{L^2}^2 + \frac{1}{\tau} \|\phi_h^{k+1} - \phi_h^k\|_{L^2}^2 - 2\langle \phi_h^{k+1} - \phi_h^k, A_h(m_h^{k+1} - m_h^k) \rangle_h.$$

The algorithm is summarized in Algorithm 1.

<sup>1</sup>The parameter choice  $\mu = \tau = 1/(2\|A_h\|)$  is convenient for complexity analysis. Practically,  $\mu = \tau = 1/\|A_h\|$  is better although it does not guarantee convergence theoretically.

---

**Algorithm 1:** A primal-dual algorithm for EMD [34]
 

---

**Input:** Distributions  $\rho^0, \rho^1$ , grid step size  $h$ , initial point  $m^0, \phi^0$ , tolerance  $\varepsilon$ .  
 Start with  $k = 0$ .  
**while**  $R_h^k < \varepsilon$  *is not satisfied* **do**  
 | Execute (3.2) and let  $k \leftarrow k + 1$ .  
**end**  
**Output:**  $m^K, \phi^K$ . ( $K$  is the number of iterations.)

---

*Algorithm 2* (Jacobs et al. [33]). Problem (2.6) can be written as:

$$(3.4) \quad \min_{m_h, u_h} \max_{\varphi_h} f(u_h) + \delta_{A_h m_h = \rho_h}(m_h) + \langle \varphi_h, m_h - u_h \rangle_h.$$

where  $\varphi_h : \Omega^h \rightarrow \mathbb{R}^d$  is the dual variable and is also the gradient of the Kantorovich potential:  $\varphi_h = A_h^* \phi_h$ . Function  $\delta_{A_h m_h = \rho_h}$  is the indicator function of  $A_h m_h = \rho_h$ :

$$\delta_{A_h m_h = \rho_h}(m_h) = \begin{cases} 0, & \text{if } A_h m_h = \rho_h, \\ +\infty, & \text{if } A_h m_h \neq \rho_h. \end{cases}$$

Define the convex conjugate of  $f$ :

$$f^*(\varphi_h) = \sup_{u_h} \langle \varphi_h, u_h \rangle_h - f(u_h).$$

Then (3.4) is equivalent to the following problem:

$$(3.5) \quad \min_{m_h} \max_{\varphi_h} \tilde{L}(m_h, \varphi_h), \quad \text{where } \tilde{L}(m_h, \varphi_h) = \delta_{A_h m_h = \rho_h}(m_h) - f^*(\varphi_h) + \langle \varphi_h, m_h \rangle_h.$$

The authors of [33] solve (3.5) in the following way:

$$(3.6) \quad \begin{aligned} m_h^{k+1} &= \arg \min_{m_h} \tilde{L}(m_h, \bar{\varphi}_h^k) + \frac{1}{2\mu} \|m_h - m_h^k\|_{L^2}^2 \\ \varphi_h^{k+1} &= \arg \max_{\varphi_h} \tilde{L}(m_h^{k+1}, \varphi_h) - \frac{1}{2\tau} \|\varphi_h - \varphi_h^k\|_{L^2}^2 \\ \bar{\varphi}_h^{k+1} &= 2\varphi_h^{k+1} - \varphi_h^k, \end{aligned}$$

where the first subproblem solving  $m_h^{k+1}$  requires computing a projection onto the affine space  $\{m_h | A_h m_h = \rho_h\}$ . Since the discrete Laplacian inverse  $((A_h)^* A_h)^{-1}$  can be easily computed by FFT, the projection could be efficiently calculated [33].

Parameters  $\mu, \tau > 0$  need to be tuned. As long as  $\mu\tau < 1$ , we have the convergence  $(m_h^k, \varphi_h^k) \rightarrow (m_h^*, \varphi_h^*)$ , where  $(m_h^*, \varphi_h^*)$  is one of the solutions of (3.5). In this paper, we choose<sup>2</sup>  $\mu = \tau = 1/2$ . The stopping condition is to have the following fixed point residual  $G^k$  small enough:

$$(3.7) \quad G_h^k = \frac{1}{\mu} \|m_h^{k+1} - m_h^k\|_{L^2}^2 + \frac{1}{\tau} \|\varphi_h^{k+1} - \varphi_h^k\|_{L^2}^2 + 2\langle \varphi_h^{k+1} - \varphi_h^k, m_h^{k+1} - m_h^k \rangle_h.$$

With  $\varphi_h^*$  in hand, the Kantorovich potential  $\phi_h^*$  can be easily found by the method given in the Appendix B. The algorithm is listed in Algorithm 2.

---

<sup>2</sup>The parameter choice  $\mu = \tau = 1/2$  is convenient for complexity analysis. Practically,  $\mu = \tau = 1$  is better.

---

**Algorithm 2:** Prox-PDHG for EMD [33]
 

---

**Input:** Distributions  $\rho^0, \rho^1$ , grid step size  $h$ , initial point  $m^0, \varphi^0$ , tolerance  $\varepsilon$ .  
 Start with  $k = 0$ .  
**while**  $G_h^k < \varepsilon$  *is not satisfied* **do**  
 | Execute (3.6) and let  $k \leftarrow k + 1$   
**end**  
**Output:**  $m^K, \varphi^K$ . ( $K$  is the number of iterations.)

---

**3.2. A framework: multilevel initialization.** In this subsection, we describe a framework, inspired by the cascadic multilevel method [12], to substantially speed up Algorithms 1 and 2. With the multilevel framework, Algorithms 1 and 2 lead to Algorithms 1M and 2M respectively.

Suppose we have  $L$  levels of grids with step sizes  $h_1, h_2, \dots, h_L$  respectively. The step sizes satisfy

$$h_1 > h_2 > \dots > h_{L-1} > h_L = h.$$

The finest step size  $h_L = h$ . On each level, the space  $\Omega$  is respectively discretized as

$$\Omega^{h_1}, \dots, \Omega^{h_{L-1}}, \Omega^{h_L}.$$

If we take  $h_l = 2^{L-l}h$ , then we have

$$\Omega^{h_1} \subset \Omega^{h_2} \subset \dots \subset \Omega^{h_{L-1}} \subset \Omega^h.$$

On the  $l^{\text{th}}$  level, the optimal flux problem (2.6) is

$$(3.8) \quad \begin{aligned} & \underset{m_{h_l}: \Omega^{h_l} \rightarrow \mathbb{R}^d}{\text{minimize}} \quad f(m_{h_l}) \\ & \text{subject to} \quad A_{h_l} m_{h_l} = \rho_{h_l}. \end{aligned}$$

We apply the cascadic multilevel technique [12] to the OT problem. We use 0 initial solution on the level  $l = 1$  and solve a sequence of minimization problem (3.8) with one pass from the coarsest level  $l = 1$  to the finest level  $l = L$ . On each level, we use Algorithm 1 or Algorithm 2 that is stopped as the iterate is accurate enough ( $R_{h_l}^k < \varepsilon_l$  for Algorithm 1,  $G_{h_l}^k < \varepsilon_l$  for Algorithm 2). The obtained solution is denoted by  $(m_{h_l}^K, \phi_{h_l}^K)$  or  $(m_{h_l}^K, \varphi_{h_l}^K)$ . After that, we interpolate the obtained solutions to the next level  $l = 2$  and treat them as the initial solutions of level  $l = 2$ . The process is repeated for  $l = 3, \dots, L$ . Algorithms 1M and 2M are the multilevel versions of Algorithms 1 and 2 respectively.

**3.3. Cross-level interpolation.** In this subsection, we describe the cross-level interpolations in Algorithms 1M and 2M in detail.

*Interpolation of potentials  $\phi_h$ .* For any  $x \in \Omega^{h_l}$  on level  $l$ , we partition the set of the coordinates  $x_j$  into two subsets, depending on whether they belong to the grid on the coarser level  $l - 1$ :

$$(3.9) \quad \begin{aligned} J_l &= \{j : x_j \in \{0, h_{l-1}, 2h_{l-1}, \dots, 1\}\}, \\ \hat{J}_l &= \{j : x_j \in \{0, h_l, 2h_l, \dots, 1\}, x_j \notin \{0, h_{l-1}, 2h_{l-1}, \dots, 1\}\}. \end{aligned}$$

Define a partial neighborhood of  $x$ :

$$\mathcal{N}_l(x) = \left\{ y \in \Omega^{h_{l-1}} : y_j = x_j, \quad \forall j \in J_l; \quad |y_j - x_j| \leq h_l, \quad \forall j \in \hat{J}_l. \right\}.$$

**Algorithm 1M** Multilevel version of Algorithm 1**Input** :  $\rho^0, \rho^1, h, L$ , a sequence of tolerances  $\{\varepsilon_l\}_{l=1}^L$ .**Initialization:** Let  $m_{h_0}^{K_0} = 0, \phi_{h_0}^{K_0} = 0$ .**for**  $l = 1, 2, \dots, L$  **do**

Initialize the current level:

$$m_{h_l}^0 = \text{Interpolate}(m_{h_{l-1}}^{K_{l-1}}), \quad \phi_{h_l}^0 = \text{Interpolate}(\phi_{h_{l-1}}^{K_{l-1}})$$

Call Algorithm 1:

$$(m_{h_l}^{K_l}, \phi_{h_l}^{K_l}) = \text{Algorithm 1}(\rho^0, \rho^1, h_l, m_{h_l}^0, \phi_{h_l}^0, \varepsilon_l)$$

**end****Output:**  $m_{h_L}^{K_L}, \phi_{h_L}^{K_L}$ **Algorithm 2M** Multilevel version of Algorithm 2**Input** :  $\rho^0, \rho^1, h, L$ , a sequence of tolerances  $\{\varepsilon_l\}_{l=1}^L$ .**Initialization:** Let  $m_{h_0}^{K_0} = 0, \varphi_{h_0}^{K_0} = 0$ .**for**  $l = 1, 2, \dots, L$  **do**

Initialize the current level:

$$m_{h_l}^0 = \text{Interpolate}(m_{h_{l-1}}^{K_{l-1}}), \quad \varphi_{h_l}^0 = \text{Interpolate}(\varphi_{h_{l-1}}^{K_{l-1}})$$

Call Algorithm 2:

$$(m_{h_l}^{K_l}, \varphi_{h_l}^{K_l}) = \text{Algorithm 2}(\rho^0, \rho^1, h_l, m_{h_l}^0, \varphi_{h_l}^0, \varepsilon_l)$$

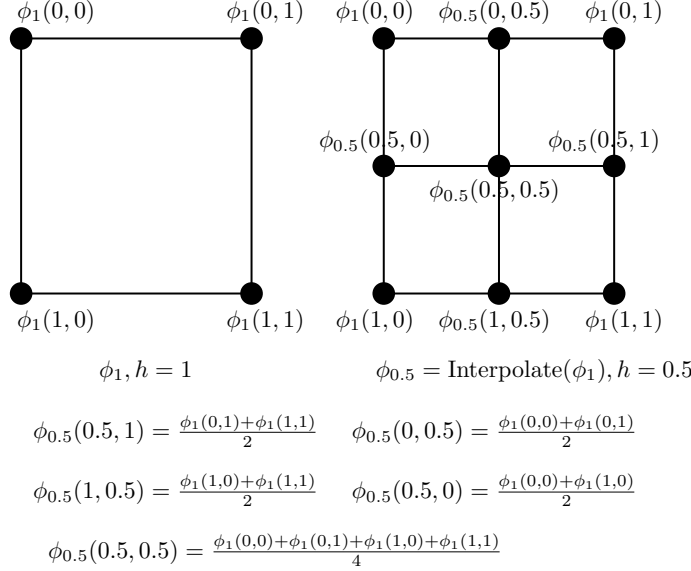
**end****Output:**  $m_{h_L}^{K_L}, \phi_{h_L}^{K_L}$  (Obtain  $\phi_{h_L}^{K_L}$  from  $\varphi_{h_L}^{K_L}$ , see Appendix B)The mapping  $\phi_{h_l} = \text{Interpolate}(\phi_{h_{l-1}})$  is defined pointwise as:

$$(3.10) \quad \phi_{h_l}(x) = \frac{1}{|\mathcal{N}_l(x)|} \sum_{y \in \mathcal{N}_l(x)} \phi_{h_{l-1}}(y), \quad \forall x \in \Omega^{h_l}.$$

For example, if  $d = 2$  (2D case) and  $h_l = 2^{-(l-1)}, l \geq 2$ , (3.10) can be written as:

$$\phi_{h_l}(x_1, x_2) = \begin{cases} \phi_{h_{l-1}}(x_1, x_2), & \text{if } (x_1, x_2) \in \mathcal{X}_1, \\ \left( \phi_{h_{l-1}}(x_1, x_2 - h_l) + \phi_{h_{l-1}}(x_1, x_2 + h_l) \right) / 2, & \text{if } (x_1, x_2) \in \mathcal{X}_2, \\ \left( \phi_{h_{l-1}}(x_1 - h_l, x_2) + \phi_{h_{l-1}}(x_1 + h_l, x_2) \right) / 2, & \text{if } (x_1, x_2) \in \mathcal{X}_3, \\ \left( \phi_{h_{l-1}}(x_1 - h_l, x_2 - h_l) + \phi_{h_{l-1}}(x_1 - h_l, x_2 + h_l) \dots \right. \\ \left. + \phi_{h_{l-1}}(x_1 + h_l, x_2 - h_l) + \phi_{h_{l-1}}(x_1 + h_l, x_2 + h_l) \right) / 4, & \text{otherwise,} \end{cases}$$

where  $\mathcal{X}_1 = \{(x_1, x_2) : x_1|_{h_{l-1}}, x_2|_{h_{l-1}}\}$ ,  $\mathcal{X}_2 = \{(x_1, x_2) : x_1|_{h_{l-1}}, x_2 \not|_{h_{l-1}}\}$  and  $\mathcal{X}_3 = \{(x_1, x_2) : x_1 \not|_{h_{l-1}}, x_2|_{h_{l-1}}\}$ . Figure 1 gives an illustration of this 2D interpolation.

FIGURE 1. An illustration of (3.10) (2D case): from  $1 \times 1$  grid to  $2 \times 2$  grid

*Interpolation of flux  $m_h$ .* Due to the zero-flux boundary condition for (2.4), interpolating  $m$  is different from  $\phi$ . The flow  $m$  can be viewed as “edge weights” on the grid [34, 4], as in Figure 2. For the  $i$ -th coordinate  $x \in \Omega_i^{h_l}$ , we use nearest neighbor interpolation:  $y_{\text{NN}} \in \arg \min_{\alpha \in \Omega_i^{h_{l-1}}} |\alpha - x_i|$ ; for the other coordinates, we use the same method with (3.10). Define a neighborhood related with direction  $i$ :

$$\hat{\mathcal{N}}_{l,i}(x) = \left\{ y \in \Omega^{h_{l-1}} : y_j = x_j, \forall j \in J_l; \quad y_i = y_{\text{NN}}; \quad |y_j - x_j| \leq h_l, \forall j \in \hat{J}_l / \{i\} \right\}$$

Then the mapping  $m_{h_l} = \text{Interpolate}(m_{h_{l-1}})$  is pointwise defined as follows:

$$(3.11) \quad m_{h_l,i}(x) = \begin{cases} \frac{1}{|\mathcal{N}_l(x)|} \sum_{y \in \mathcal{N}_l(x)} m_{h_{l-1},i}(y), & i \in J_l, \\ \frac{1}{|\hat{\mathcal{N}}_{l,i}(x)|} \sum_{y \in \hat{\mathcal{N}}_{l,i}(x)} m_{h_{l-1},i}(y), & i \in \hat{J}_l. \end{cases}$$

For example, if  $d = 2$  (2D case) and  $h_l = 2^{-(l-1)}$ ,  $l \geq 2$ , (3.11) can be written as:

$$m_{h_l,1}(x_1, x_2) = \begin{cases} m_{h_{l-1},1}(x_1, x_2), & \text{if } (x_1, x_2) \in \mathcal{X}_1, \\ m_{h_{l-1},1}(x_1 - h_l, x_2), & \text{if } (x_1, x_2) \in \mathcal{X}_3, \\ \left( m_{h_{l-1},1}(x_1, x_2 - h_l) + m_{h_{l-1},1}(x_1, x_2 + h_l) \right) / 2, & \text{if } (x_1, x_2) \in \mathcal{X}_2, \\ \left( m_{h_{l-1},1}(x_1 - h_l, x_2 - h_l) + m_{h_{l-1},1}(x_1 - h_l, x_2 + h_l) \right) / 2, & \text{otherwise,} \end{cases}$$

$$m_{h_l,2}(x_1, x_2) = \begin{cases} m_{h_{l-1},2}(x_1, x_2), & \text{if } (x_1, x_2) \in \mathcal{X}_1, \\ m_{h_{l-1},2}(x_1, x_2 - h_l), & \text{if } (x_1, x_2) \in \mathcal{X}_2, \\ \left( m_{h_{l-1},2}(x_1 - h_l, x_2) + m_{h_{l-1},2}(x_1 + h_l, x_2) \right) / 2, & \text{if } (x_1, x_2) \in \mathcal{X}_3, \\ \left( m_{h_{l-1},2}(x_1 - h_l, x_2 - h_l) + m_{h_{l-1},2}(x_1 + h_l, x_2 - h_l) \right) / 2, & \text{otherwise.} \end{cases}$$

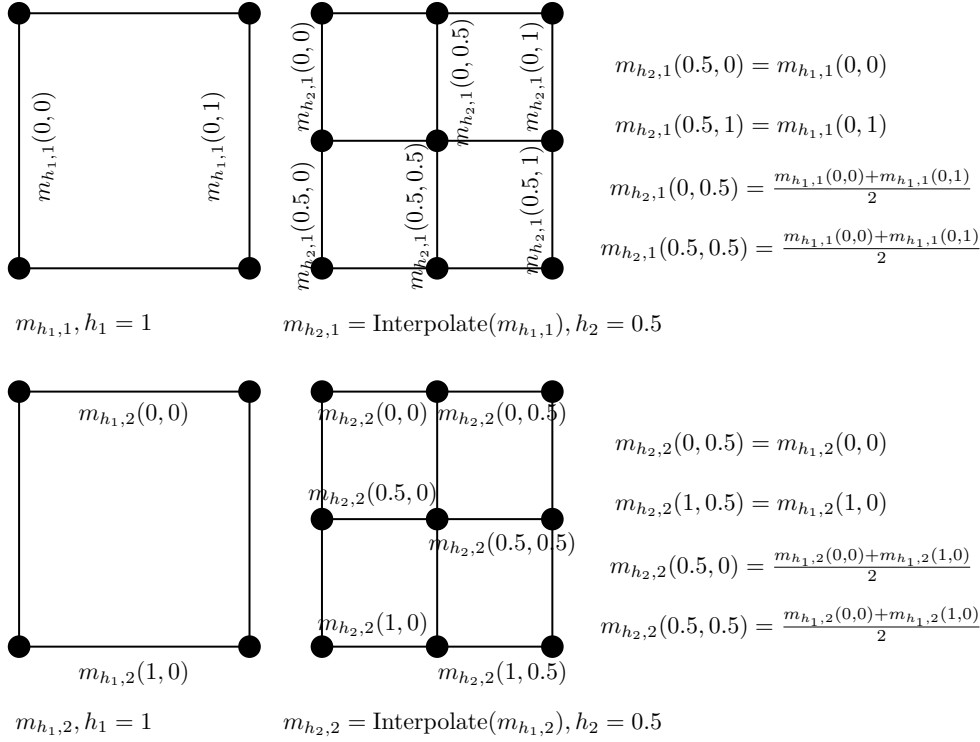
FIGURE 2. An illustration of (3.11) (2D case): from  $1 \times 1$  grid to  $2 \times 2$  grid

Figure 2 illustrates the above formula.

*Interpolation of  $\varphi_h$ .* Since  $\varphi_h$  has the same dimension as  $m_h$ , the interpolation of  $\varphi_h$  is the same as interpolation of flux  $m_h$  (3.11).

The interpolation operators introduced above are linear operators satisfying the following properties that are proved in Appendix A:

LEMMA 3.1. *If  $h_{l-1} = 2h_l$ , then we have*

$$(3.12) \quad \begin{aligned} \|\text{Interpolate}(\phi_{h_{l-1}})\|_{L^2}^2 &\leq \|\phi_{h_{l-1}}\|_{L^2}^2, & \forall \phi_{h_{l-1}} : \Omega^{h_{l-1}} &\rightarrow \mathfrak{R}. \\ \|\text{Interpolate}(m_{h_{l-1}})\|_{L^2}^2 &\leq \|m_{h_{l-1}}\|_{L^2}^2, & \forall m_{h_{l-1}} : \Omega^{h_{l-1}} &\rightarrow \mathfrak{R}^d. \\ \|\text{Interpolate}(\varphi_{h_{l-1}})\|_{L^2}^2 &\leq \|\varphi_{h_{l-1}}\|_{L^2}^2, & \forall \varphi_{h_{l-1}} : \Omega^{h_{l-1}} &\rightarrow \mathfrak{R}^d. \end{aligned}$$

**3.4. Parameter choices.** The choice of stopping tolerances ( $\varepsilon$  for Algorithms 1 and 2;  $\{\varepsilon_l\}_{l=1}^L$  for Algorithms 1M and 2M) are critical to the practical performances of the algorithms. We will discuss the theoretical conditions for the tolerances in Section 4 and empirical formulas in Section 6. To summarize, we list typical rules in 2D ( $d = 2$ ) case below:

- Algorithm 1:  $\varepsilon = O(h^3)$ .
- Algorithm 2:  $\varepsilon = O(h^2)$ .
- Algorithm 1M:  $\varepsilon_l = \varepsilon_L \times (h_l/h_L)^{-1}$ , where  $\varepsilon_L = O(h^2)$ .
- Algorithm 2M:  $\varepsilon_l = \varepsilon_L \times (h_l/h_L)^{-1}$ , where  $\varepsilon_L = O(h^2)$ .

With these rules, the algorithms provide outputs with errors in the order of the discretization error. Moreover, we take  $L = O(\log(1/h))$ .

**4. Analysis of computational costs.** In this section, we provide a complexity analysis of Algorithms 1, 2, 1M and 2M. We introduce compact notions  $z_h = (m_h, \phi_h)$  for Algorithms 1, 1M and  $y_h = (m_h, \varphi_h)$  for Algorithms 2, 2M. Let  $Z_h^*, Y_h^*$ , respectively, be the solution set of the following min-max problems with grid step size  $h$ :

$$\begin{aligned} Z_h^* &= \left\{ (m_h^*, \phi_h^*) \mid (m_h^*, \phi_h^*) \text{ is a saddle point of } L(m_h, \phi_h) \right\}, \\ Y_h^* &= \left\{ (m_h^*, \varphi_h^*) \mid (m_h^*, \varphi_h^*) \text{ is a saddle point of } \tilde{L}(m_h, \varphi_h) \right\}, \end{aligned}$$

where  $L$  and  $\tilde{L}$  are defined in (3.1) and (3.5) respectively.

**4.1. Assumptions.** In this subsection, some assumptions used in our theories will be introduced and discussed.

ASSUMPTION 1. *The solution sets  $Z_{h_l}^*$  on all the levels are nonempty. And there exists a constant  $C_1$  independent of  $h_l$  such that,*

$$(4.1) \quad \|z_{h_l}^*\|_{L^2}^2 \leq C_1, \quad \forall z_{h_l}^* \in Z_{h_l}^*, \quad l = 1, 2, \dots, L.$$

Assumption 1 is mild. Since  $z_{h_l}^* = (m_{h_l}^*, \phi_{h_l}^*)$ , the norm of  $z_{h_l}^*$  can be decomposed as  $\|z_{h_l}^*\|_{L^2}^2 = \|m_{h_l}^*\|_{L^2}^2 + \|\phi_{h_l}^*\|_{L^2}^2$ . The dual solution  $\phi_{h_l}^*$ , by the definition in (2.7), has the property:  $\|A_h^* \phi_{h_l}^*(x)\|_q \leq 1, \forall x \in \Omega^{h_l}$ , where  $A_h^*$  is the gradient operator defined on  $\Omega^{h_l}$ . It implies that all the dual solutions  $\phi_{h_l}^*$  are Lipschitz continuous uniformly on the compact domain  $\Omega = [0, 1]^d$ . Thus, all the dual solutions  $\phi_{h_l}^*$  are uniformly bounded as long as they are kept with a zero mean. Actually keeping  $\phi_{h_l}^*$  to be zero-meaned is not difficult, see [54]. The primal solution  $m_{h_l}^*$ , by definition, is the solution of minimization problem (3.8). It suffices to have  $L^2$ -boundedness of  $m_{h_l}^*$  if  $\rho^0, \rho^1$  are smooth. In that case,  $\rho_{h_l}^0, \rho_{h_l}^1$  are similar on different levels and so does  $m_{h_l}^*$ , then (4.1) can be expected. Generally speaking, on some extreme cases like  $\rho^0$  and  $\rho^1$  are  $\delta$ -functions, it does not hold. However, on commonly used examples, we numerically validated Assumption 1 in Table 3 and observed that  $C_1$  exists and is independent of grid size.

ASSUMPTION 2. *For any optimal solution  $z_{h_l}^* \in Z_{h_l}^*$  on level  $l$ , there exists an optimal solution  $z_{h_{l+1}}^* \in Z_{h_{l+1}}^*$  on the finer level  $l+1$  such that*

$$(4.2) \quad \|\text{Interpolate}(z_{h_l}^*) - z_{h_{l+1}}^*\|_{L^2}^2 \leq C_2 (h_l)^r, \quad l = 1, 2, \dots, L-1,$$

where  $C_2 > 0$  is independent of  $h_l$  and  $r > 0$  depends on the smoothness of the solution  $z_{h_l}^*$ , the interpolation method we choose and the properties of  $\rho_{h_l}^0$  and  $\rho_{h_l}^1$  on each of the levels.

Assumption 2 requires the solution sets between two consecutive levels are close to each other and each solution is smooth enough. Ideally speaking, if  $z_{h_l}^*$  and  $z_{h_{l+1}}^*$  are the discretized version of the same underlying continuous  $z^*$  and  $z^*$  is smooth enough, it should hold  $r = 2$  due to our interpolation method. Generally speaking, one can only expect  $z_h^* \rightarrow z^*$  as  $h \rightarrow 0$  without knowing the convergence rate [9] and the smoothness of  $z^*$  cannot be guaranteed (for example,  $\rho^0$  and  $\rho^1$  are taken as  $\delta$ -functions). Thus, we are not able to show (4.2) holds theoretically. However, Assumption 2 holds on commonly used examples. We numerically validated it in Section 5.1 with  $d = 2$  and  $p = 1, 2, \infty$ . Figures 3 and 4 give a visualized example that has multiple solutions on different levels. Table 3 quantifies  $\|\text{Interpolate}(z_{h_l}^*) - z_{h_{l+1}}^*\|_{L^2}^2$  and shows that  $r$  is approximately  $r \approx 2$ .

ASSUMPTION 3. *The solution sets  $Y_{h_l}^*$  on all the levels are nonempty. And there exists a constant  $C_3$  independent of  $h_l$  such that,*

$$(4.3) \quad \|y_{h_l}^*\|_{L^2}^2 \leq C_3, \quad \forall y_{h_l}^* \in Y_{h_l}^*, \quad l = 1, 2, \dots, L.$$

Similar with the discussion following Assumption 1,  $\|y_{h_l}^*\|_{L^2}^2 = \|m_{h_l}^*\|_{L^2}^2 + \|\varphi_{h_l}^*\|_{L^2}^2$ . The dual optimal solution  $\varphi_{h_l}^*$ , by the definition in (3.5), has the property:  $\varphi_{h_l}^* = A_h^* \phi_{h_l}^*$ . Since  $\|A_h^* \phi_{h_l}^*(x)\|_q \leq 1, \forall x \in \Omega^{h_l}$ , we have  $\|\varphi_{h_l}^*(x)\|_q \leq 1, \forall x \in \Omega^{h_l}$ , which implies all the dual solutions  $\phi_{h_l}^*$  are uniformly bounded:<sup>3</sup>

$$\|\varphi_{h_l}^*\|_{L^2}^2 = \sum_{x \in \Omega^{h_l}} \|\varphi_{h_l}^*(x)\|_2^2 h_l^d \leq \sum_{x \in \Omega^{h_l}} d \|\varphi_{h_l}^*(x)\|_q^2 h_l^d \leq d.$$

ASSUMPTION 4. *For any optimal solution  $y_{h_l}^* \in Y_{h_l}^*$  on level  $l$ , there exists an optimal solution  $y_{h_{l+1}}^* \in Y_{h_{l+1}}^*$  on the finer level  $l+1$  such that*

$$(4.4) \quad \|\text{Interpolate}(y_{h_l}^*) - y_{h_{l+1}}^*\|_{L^2}^2 \leq C_4 (h_l)^\nu, \quad l = 1, 2, \dots, L-1,$$

where  $C_4 > 0$  is independent of  $h_l$  and  $\nu > 0$  depends on the smoothness of the solution  $y_{h_l}^*$ , the interpolation method we choose and the properties of  $\rho_{h_l}^0$  and  $\rho_{h_l}^1$  on each of the levels.

Table 3 shows that  $\nu$  is approximately  $\nu \approx 1$  on the commonly used examples. The factor  $\nu$  is smaller than the factor  $r$  in Assumption 2 ( $r \approx 2$  on the same examples) because  $\varphi_{h_l}^*$  is the gradient of  $\phi_{h_l}^*$ :  $\varphi_{h_l}^* = A_h^* \phi_{h_l}^*$  and  $\varphi_{h_l}^*$  is less smooth than  $\phi_{h_l}^*$ . Figures 4 and 6 visualize  $\phi_{h_l}^*$  and  $\varphi_{h_l}^*$  respectively and support this point.

**4.2. Analysis of Algorithms 1 and 1M.** Assumption (4.2) tells us the solution on the  $l$ -th level  $z_{h_l}^*$  has an grid error up to  $O((h_l)^r)$  compared with the solution on a finer level  $z_{h_{l+1}}^*$ . Thus, on each level, it's enough to do iteration until  $\|z_{h_l}^{K_l} - z_{h_l}^*\|_{L^2}^2 \leq O((h_l)^r)$ . The following lemma demonstrates that, as long as we choose  $\varepsilon$  (for Algorithm 1) and  $\{\varepsilon_l\}_{l=1}^L$  (for Algorithm 1M) properly, such condition can be satisfied.

LEMMA 4.1. *Given  $\rho^0, \rho^1, h$ , we choose  $h_l = 2^{L-l}h$ .*

1. *There exists  $\bar{\varepsilon}$ , as long as we run Algorithm 1 with any  $\varepsilon \leq \bar{\varepsilon}$ , we have*

$$(4.5) \quad \|z_h^K - z_h^*\|_{L^2}^2 \leq C_2 h^r, \quad \text{for some } z_h^* \in Z_h^*.$$

2. *Suppose we run Algorithm 1M with arbitrary tolerances  $\{\varepsilon_i\}_{i=1}^{l-1}$  on the lowest  $l-1$  levels. There exists a threshold  $\bar{\varepsilon}_l$  depending on  $\{\varepsilon_i\}_{i=1}^{l-1}$ , as long as we set  $\varepsilon_l \leq \bar{\varepsilon}_l \left( \{\varepsilon_i\}_{i=1}^{l-1} \right)$  on level  $l$ , we have*

$$(4.6) \quad \|z_{h_l}^{K_l} - z_{h_l}^*\|_{L^2}^2 \leq C_2 (h_l)^r, \quad \text{for some } z_{h_l}^* \in Z_{h_l}^*.$$

*Proof. Step 1:* We consider Algorithm 1. Define

$$M_h = h^d \begin{bmatrix} I/\mu & -(A_h)^* \\ -A_h & I/\tau \end{bmatrix}.$$

<sup>3</sup>This bound is due to the fact that  $\|a\|_2 \leq \sqrt{d}\|a\|_q$  for all  $a \in \mathfrak{R}^d$  and  $1 \leq q \leq \infty$ .

Then the fixed point residual can be written as  $R_h^k = \|z_h^{k+1} - z_h^k\|_{M_h}^2$ , and Chambolle-Pock is equivalent to the proximal point algorithm (PPA) with the  $M_h$ -metric (Theorem 1 in [34]). Given  $\mu\tau\|A_h\|^2 < 1$ ,  $R_h^k$  is monotone:

$$(4.7) \quad R_h^{k+1} \leq R_h^k, \quad \forall k,$$

and the global convergence holds in the sense:

$$(4.8) \quad z_h^k \rightarrow z_h^*, \quad \text{for some } z_h^* \in Z_h^*, \text{ as } k \rightarrow \infty.$$

The global convergence (4.8) means that there exists a  $\bar{K}$ , such that  $\|z_h^k - z_h^*\|_{L^2}^2 \leq C_2 h^r$  holds for all  $k \geq \bar{K}$ . Let  $\bar{\varepsilon} = R_h^{\bar{K}}$  and  $K$  be the number of iterations when the stopping condition  $R_h^K \leq \varepsilon$  is satisfied. As long as  $\varepsilon < \bar{\varepsilon}$ , we have

$$R_h^K \leq \varepsilon < \bar{\varepsilon} = R_h^{\bar{K}}.$$

Then, by the monotonicity of FPR (4.7), we conclude that  $K \geq \bar{K}$ . Inequality (4.5) is proved.

**Step 2:** Next we consider Algorithm 1M. On the first level  $l = 1$ , we repeat the same argument as above, and we obtain that, there exists a threshold  $\bar{\varepsilon}_1$  such that (4.6) holds for  $l = 1$  as long as  $\varepsilon_1 \leq \bar{\varepsilon}_1$ . Similarly, for  $l \geq 2$ , there exists a threshold  $\bar{\varepsilon}_l$  such that (4.6) holds for  $l \geq 2$  as long as  $\varepsilon_l \leq \bar{\varepsilon}_l$ . Now let's analyze the dependencies of  $\bar{\varepsilon}_l$  and  $\{\varepsilon_i\}_{i=1}^{l-1}$ . Suppose  $\{\varepsilon_i\}_{i=1}^{l-1}$  are given. By running Algorithm 1M on level  $1, 2, \dots, l-1$ , we are able to determine the solution of the  $(l-1)$ -th level  $z_{h_{l-1}}^{K_{l-1}}$ . Conducting interpolation on  $z_{h_{l-1}}^{K_{l-1}}$ , we obtain  $z_{h_l}^0$ . In another word,  $z_{h_l}^0$  is determined by the threshold sequence  $\{\varepsilon_i\}_{i=1}^{l-1}$ . Since  $\bar{\varepsilon}_l$  depends on  $z_{h_l}^0$  and  $z_{h_l}^0$  depends on  $\{\varepsilon_i\}_{i=1}^{l-1}$ , we can write  $\bar{\varepsilon}_l$  as a function of  $\{\varepsilon_i\}_{i=1}^{l-1}$ :  $\bar{\varepsilon}_l(\{\varepsilon_i\}_{i=1}^{l-1})$ . For any  $\varepsilon_l \leq \bar{\varepsilon}_l(\{\varepsilon_i\}_{i=1}^{l-1})$ , (4.6) holds. Lemma 4.1 is proved.  $\square$

We define the set of ‘‘good’’ stopping tolerances for Algorithms 1 and 1M:

$$(4.9) \quad \mathcal{T}_1 = \left\{ \varepsilon \mid \varepsilon \leq \bar{\varepsilon} \right\},$$

$$(4.10) \quad \mathcal{T}_{1M} = \left\{ \{\varepsilon_l\}_{l=1}^L \mid \varepsilon_1 \leq \bar{\varepsilon}_1, \varepsilon_2 \leq \bar{\varepsilon}_2(\varepsilon_1), \dots, \varepsilon_L \leq \bar{\varepsilon}_L(\{\varepsilon_l\}_{l=1}^{L-1}) \right\}.$$

Based on Lemma 4.1,  $\mathcal{T}_1$  and  $\mathcal{T}_{1M}$  are nonempty. Given these stopping tolerances, the performance of Algorithms 1 and 1M can be analyzed as follows.

**THEOREM 4.2.** *Given  $\rho^0, \rho^1, h, L \geq 2$  and  $h_l = 2^{L-l}h$  and Assumptions 1,2, if we take 0 as the initialization, then the following holds<sup>4</sup>:*

1. *With  $\varepsilon \in \mathcal{T}_1$ , Algorithm 1 takes  $O(\frac{1}{\varepsilon} \frac{\sqrt{d}}{h})$  iterations to stop.*
2. *With  $\{\varepsilon_l\}_{l=1}^L \in \mathcal{T}_{1M}$ , Algorithm 1M takes  $O(\frac{1}{\varepsilon_l} \frac{\sqrt{d}}{h_l^{1-r}})$  iterations on level  $l$  ( $l \geq 2$ ).*

This theorem shows why Algorithm 1M helps speed up Algorithm 1. As long as the optimal solution on the coarse level is close to one of the optimal solutions on the finer level, the multilevel technique is able to reduce the number of iterations on the finer level. If the distance between the coarse solution and the fine solution is

<sup>4</sup>In this article,  $O(\cdot)$  denotes the asymptotic rate as  $\varepsilon \rightarrow 0$  and  $h \rightarrow 0$ .

controlled by  $O(h^r)$  (Assumption 2), the number of iterations can be reduced by  $h^r$ . Specifically, with  $\varepsilon = \varepsilon_L$ , Algorithm 1 takes  $O(\frac{1}{\varepsilon} \frac{\sqrt{d}}{h})$  iterations while Algorithm 1M takes  $O(\frac{1}{\varepsilon} \frac{\sqrt{d}}{h^{1-\tau}})$  on the finest level because  $h = h_L$ . Although Algorithm 1M leads to extra calculations on coarser grids, the advantage of our multilevel algorithm is able to overcome the extra costs. Table 4 validates this point. Moreover, the choice of  $\varepsilon = \varepsilon_L$  is reasonable, even over-fair, in practice. Table 5 shows that Algorithm 1M can obtain better solution than Algorithm 1 with  $\varepsilon_L > \varepsilon$ .

*Proof. Step 1:* Analyzing how many iterations Algorithm 1 takes. As we discussed in the proof of Lemma 4.1, Algorithm 1 is equivalent to PPA with the  $M_h$ -metric. By [31], we have:

$$(4.11) \quad R_h^k \leq \frac{1}{k} \|z_h^0 - z_h^*\|_{M_h}^2, \quad \forall z_h^* \in Z_h^*.$$

The definition of  $M_h$  gives us

$$\|z_h^0 - z_h^*\|_{M_h}^2 = h^d \left( \frac{1}{\mu} \|m_h^0 - m_h^*\|_2^2 + \frac{1}{\tau} \|\phi_h^0 - \phi_h^*\|_2^2 - 2\langle \phi_h^0 - \phi_h^*, A_h(m_h^0 - m_h^*) \rangle \right),$$

where the last term of the right hand side can be bounded by applying the Peter–Paul inequality  $2\langle x, y \rangle \leq \|x\|_2^2/\epsilon + \epsilon\|y\|_2^2$  with  $x = -(\phi_h^0 - \phi_h^*)$ ,  $y = A_h(m_h^0 - m_h^*)$  and  $\epsilon = 1/\|A_h\|$ :

$$-2\langle \phi_h^0 - \phi_h^*, A_h(m_h^0 - m_h^*) \rangle \leq \|A_h\| \cdot \|\phi_h^0 - \phi_h^*\|_2^2 + \|A_h\| \cdot \|m_h^0 - m_h^*\|_2^2.$$

Given the parameter choice  $\mu = \tau = 1/(2\|A_h\|)$ , we obtain the following bound

$$\begin{aligned} \|z_h^0 - z_h^*\|_{M_h}^2 &= 2h^d \left( \|A_h\| \left( \|m_h^0 - m_h^*\|_2^2 + \|\phi_h^0 - \phi_h^*\|_2^2 \right) - \langle \phi_h^0 - \phi_h^*, A_h(m_h^0 - m_h^*) \rangle \right) \\ &\leq 3\|A_h\| h^d \left( \|m_h^0 - m_h^*\|_2^2 + \|\phi_h^0 - \phi_h^*\|_2^2 \right) \\ &\leq 3\|A_h\| \|z_h^0 - z_h^*\|_{L^2}^2. \end{aligned}$$

The norm  $\|A_h\|$  is the square root of the largest singular-value of  $(A_h)^*A_h$ , which is the discrete Laplacian with grid step size  $h$ . By the Gershgorin circle theorem [27],  $\sigma_{\max}((A_h)^*A_h) \leq 4\frac{d}{h^2}$  and, thus,  $\|A_h\| \leq 2\frac{\sqrt{d}}{h}$ , which implies

$$(4.12) \quad \|z_h^0 - z_h^*\|_{M_h}^2 \leq 6\frac{\sqrt{d}}{h} \|z_h^0 - z_h^*\|_{L^2}^2.$$

Since we take zero as the initialization  $z_h^0 = 0$ , based on Assumption 1, we have

$$(4.13) \quad \|z_h^0 - z_h^*\|_{L^2}^2 = \|z_h^*\|_{L^2}^2 \leq C_1.$$

Inequalities (4.11), (4.12) and (4.13) imply

$$(4.14) \quad R_h^k \leq \frac{1}{k} \|z_h^0 - z_h^*\|_{M_h}^2 \leq 6\sqrt{d} \frac{1}{kh} \|z_h^0 - z_h^*\|_{L^2}^2 \leq 6\sqrt{d} \frac{1}{kh} C_1.$$

As long as  $k > 6C_1 \frac{1}{\varepsilon} \frac{\sqrt{d}}{h}$ , the stopping condition  $R_h^k < \varepsilon$  is satisfied. Algorithm 1 stops within  $(6C_1 \frac{1}{\varepsilon} \frac{\sqrt{d}}{h}) \approx O(\frac{1}{\varepsilon} \frac{\sqrt{d}}{h})$  iterations, i.e.,  $K = O(\frac{1}{\varepsilon} \frac{\sqrt{d}}{h})$ .

**Step 2:** Analyzing how many iterations Algorithm 1M takes on level  $l$  ( $l \geq 2$ ).

Similar to (4.11) and (4.12), on level  $l$ , it holds that

$$R_{h_l}^k \leq \frac{1}{k} \|z_{h_l}^0 - z_{h_l}^*\|_{M_{h_l}}^2 \leq \frac{6\sqrt{d}}{kh_l} \|z_{h_l}^0 - z_{h_l}^*\|_{L^2}^2.$$

The distance in the right hand side can be bounded by

$$\begin{aligned} \|z_{h_l}^0 - z_{h_l}^*\|_{L^2}^2 &= \|\text{Interpolate}(z_{h_{l-1}}^{K_{l-1}}) - z_{h_l}^*\|_{L^2}^2 \\ &\leq 2 \underbrace{\left\| \text{Interpolate}(z_{h_{l-1}}^{K_{l-1}}) - \text{Interpolate}(z_{h_{l-1}}^*) \right\|_{L^2}^2}_{\text{T1}} + 2 \underbrace{\left\| \text{Interpolate}(z_{h_{l-1}}^*) - z_{h_l}^* \right\|_{L^2}^2}_{\text{T2}}, \end{aligned}$$

where the first term can be bounded by

$$\text{T1} = 2 \|\text{Interpolate}(z_{h_{l-1}}^{K_{l-1}} - z_{h_{l-1}}^*)\|_{L^2}^2 \leq 2 \|z_{h_{l-1}}^{K_{l-1}} - z_{h_{l-1}}^*\|_{L^2}^2$$

because the ‘‘interpolate’’ operator is linear and nonexpansive by Lemma 3.1. Furthermore, due to Lemma 4.1 and the assumption that  $\{\varepsilon_l\}_{l=1}^L \in \mathcal{T}_{1M}$ , we have

$$\text{T1} \leq 2 \|z_{h_{l-1}}^{K_{l-1}} - z_{h_{l-1}}^*\|_{L^2}^2 \leq 2C_2(h_{l-1})^r.$$

The second term T2 can be bounded with Assumption 2:  $\text{T2} \leq 2C_2(h_{l-1})^r$ . Thus, for Algorithm 1M, we can obtain a better bound than (4.13):

$$\|z_{h_l}^0 - z_{h_l}^*\|_{L^2}^2 \leq \text{T1} + \text{T2} \leq 4C_2(h_{l-1})^r = 4C_2(2h_l)^r.$$

All the results above implies

$$(4.15) \quad R_{h_l}^k \leq \frac{6\sqrt{d}}{kh_l} \|z_{h_l}^0 - z_{h_l}^*\|_{L^2}^2 \leq \frac{6\sqrt{d}}{kh_l} 4C_2(2h_l)^r = 24 \cdot 2^r C_2 \frac{\sqrt{d}}{h_l^{1-r}} \frac{1}{k}.$$

As long as  $k > 24 \cdot 2^r C_2 \frac{\sqrt{d}}{h_l^{1-r}} \frac{1}{\varepsilon_l}$ , we have  $R_{h_l}^k \leq \varepsilon_l$ , i.e., the stopping condition on level  $l$  is satisfied. Thus the number of iterations on level  $l$  can be bounded by  $K_l \leq 24 \cdot 2^r C_2 \frac{\sqrt{d}}{h_l^{1-r}} \frac{1}{\varepsilon_l} = O(\frac{1}{\varepsilon_l} \frac{\sqrt{d}}{h_l^{1-r}})$ . Theorem 4.3 is proved.  $\square$

Theorem 4.2 shows that the stopping tolerances in the sets  $\mathcal{T}_1$  and  $\mathcal{T}_{1M}$  are good choices. However, the conditions (4.9) and (4.10) are intractable to check during we run the algorithms. Here we propose an explicit empirical formula for choosing  $\{\varepsilon_l\}_{l=1}^L$ :

$$(4.16) \quad \varepsilon_l = \varepsilon_L \times \left(\frac{h_l}{h}\right)^\alpha, \quad \alpha \in \mathfrak{R},$$

where  $\varepsilon_L$  is the stopping tolerance for the highest level  $l = L$ . With (4.16), we provide the complexity analysis of Algorithms 1 and 1M below.

**THEOREM 4.3.** *Given  $\rho^0, \rho^1, h, h_l = 2^{L-l}h$  and Assumptions 1,2, if we take 0 as the initialization, the following holds:*

1. With  $\varepsilon \in \mathcal{T}_1$ , the complexity of Algorithm 1 is

$$(4.17) \quad \mathcal{O}_1 = O\left(\frac{1}{\varepsilon} \frac{d^{3/2}}{h^{d+1}}\right).$$

2. With  $\{\varepsilon_l\}_{l=1}^L$  chosen by (4.16) and  $\{\varepsilon_l\}_{l=1}^L \in \mathcal{T}_{1M}$  and  $L = 1 + \log_2(1/h)$ , the complexity of Algorithm 1M is

$$(4.18) \quad \mathcal{O}_{1M} = \begin{cases} O\left(\frac{1}{\varepsilon_L} \frac{d^{3/2}}{h^{d+1-r}}\right) + O\left(\frac{d2^d}{h^d}\right), & \text{if } \alpha > r - d - 1, \\ O\left(\frac{1}{\varepsilon_L} \frac{d^{3/2}}{h^{d+1-r}} \log\left(\frac{1}{h}\right)\right) + O\left(\frac{d2^d}{h^d}\right), & \text{if } \alpha = r - d - 1, \\ O\left(\frac{1}{\varepsilon_L} \frac{d^{3/2}}{h^{-\alpha}}\right) + O\left(\frac{d2^d}{h^d}\right), & \text{if } \alpha < r - d - 1. \end{cases}$$

Theorem 4.3 shows that, if  $\{\varepsilon_l\}_{l=1}^L \in \mathcal{T}_{1M}$ , we should choose a large  $\alpha$  to enjoy better complexity. A small  $\alpha$  leads to small tolerance on lower levels  $l < L$  and extra computational burdens on those levels. This is why  $\mathcal{O}_{1M}$  has a worse bound  $h^\alpha$  as  $\alpha < r - d - 1$ . However, to guarantee  $\{\varepsilon_l\}_{l=1}^L \in \mathcal{T}_{1M}$  in practice, we have to choose smaller  $\varepsilon_L$  if we choose larger  $\alpha$ . Then it will cost more calculations on the highest level, which hurts the advantage of multilevel methods. Thus, we should choose a proper  $\alpha$  and make balance between the computations on lower and higher levels. In Table 5, we will numerically test this point.

*Proof.* First, we consider the case where  $p = 1$  or  $p = 2$ .

For Algorithm 1, the complexity is “iterations  $\times$  single step complexity.” In each step of Algorithm 1, the dominant calculation is computing  $A_h m_h$  or  $(A_h)^* \phi_h$  [34], which has a complexity of  $O\left(\frac{d}{h^d}\right)$ . Thus, the total complexity of Algorithm 1 is:

$$\mathcal{O}_1 = O\left(\frac{1}{\varepsilon} \frac{\sqrt{d}}{h}\right) \times O\left(\frac{d}{h^d}\right) = O\left(\frac{1}{\varepsilon} \frac{d^{3/2}}{h^{d+1}}\right).$$

For Algorithm 1M, the complexity is the sum of two parts: iterations on all levels  $\mathcal{O}_{1M,1}$  and the interpolations between the levels  $\mathcal{O}_{1M,2}$ . Let us first consider the former part. Similar to Algorithm 1, the complexity of level 1 is  $O\left(\frac{1}{\varepsilon_1} \frac{d^{3/2}}{h_1^{d+1}}\right)$ . The complexity of Level  $l$  ( $2 \leq l \leq L$ ) is  $O\left(\frac{1}{\varepsilon_l} \frac{d^{3/2}}{h_l^{d+1-r}}\right)$ . Given  $h_l = 2^{L-l}h$  and  $L = 1 + \log_2(1/h)$ , it holds that  $h_l = 2^{-(l-1)}$ . Due to (4.16), we are able to obtain:

$$\begin{aligned} \mathcal{O}_{1M,1} &= \sum_{l=2}^L O\left(\frac{1}{\varepsilon_l} \frac{d^{3/2}}{h_l^{d+1-r}}\right) + O\left(\frac{1}{\varepsilon_1} \frac{d^{3/2}}{h_1^{d+1}}\right) = O\left(\frac{h^\alpha}{\varepsilon_L}\right) \left(\sum_{l=2}^L \frac{d^{3/2}}{h_l^{d+1+\alpha-r}} + \frac{d^{3/2}}{h_1^{d+1+\alpha}}\right) \\ &= O\left(\frac{1}{\varepsilon_L} \frac{d^{3/2}}{h^{d+1-r}}\right) \left(\sum_{i=0}^{L-2} 2^{-i(d+1+\alpha-r)} + 2^{-(d+1+\alpha)(L-1)} h^{-r}\right) \\ &= O\left(\frac{1}{\varepsilon_L} \frac{d^{3/2}}{h^{d+1-r}}\right) \left(\sum_{i=0}^{L-1} 2^{-i(d+1+\alpha-r)}\right). \end{aligned}$$

We consider three cases:

- If  $\alpha > r - d - 1$ , we have  $\sum_{i=0}^{L-1} 2^{-i(d+1+\alpha-r)} < \infty$  is a constant.
- If  $\alpha = r - d - 1$ , we have  $\sum_{i=0}^{L-1} 2^{-i(d+1+\alpha-r)} = L$ .
- If  $\alpha < r - d - 1$ , we have  $\sum_{i=0}^{L-1} 2^{-i(d+1+\alpha-r)} = O(2^{L(r-d-1-\alpha)})$ .

Then  $\mathcal{O}_{1M,1}$  is obtained.

Now let us consider the second part, the complexity of interpolations between the levels  $l$  and  $l + 1$ . Each node on level  $l + 1$  is obtained by no more than  $2^d$  nodes, totally we have  $O(d/h_{l+1}^d)$  nodes, so the complexity of interpolation between the levels  $l$  and  $l + 1$  is  $O(d2^d/h_{l+1}^d)$ . Summing them up,

$$\mathcal{O}_{1M,2} = O\left(\frac{d2^d}{h^d}\right) \left(1 + \frac{1}{2^d} + \frac{1}{2^{2d}} + \cdots + \frac{1}{2^{(L-1)d}}\right) = O\left(\frac{d2^d}{h^d}\right).$$

For  $p = \infty$ , the dominant calculation in a single step includes two parts. One is computing  $A_h m_h$  or  $(A_h)^* \phi_h$ , which is the same with the case of  $p = 1, 2$ . The other is calculating the  $\ell_\infty$  shrinkage operator. By the Moreau decomposition [40], computing an  $\ell_\infty$  shrinkage operator is equivalent with computing a projection onto an  $\ell_1$  ball. By [21], the complexity of the latter is  $O(d)$ . We need to project all the points  $x \in \Omega^h$ . In total, there are  $O(N^d) = O(1/h^d)$  points, so the single step complexity is  $O(\frac{d}{h^d})$ . Following the above argument, we obtain the complexities of Algorithm 1 and Algorithm 1M as  $p = \infty$  have the same asymptotic rate as  $p = 1, 2$ .  $\square$

**4.3. Analysis of Algorithms 2 and 2M.** Similar to Lemma 4.1, we establish the conditions of stopping tolerances for Algorithms 2 and 2M.

LEMMA 4.4. *Given  $\rho^0, \rho^1, h$ , we assume  $h_l = 2^{L-l}h$ .*

1. *There exists  $\tilde{\varepsilon}$ , as long as we run Algorithm 2 with  $\varepsilon \leq \tilde{\varepsilon}$ , we have*

$$(4.19) \quad \|y_h^K - y_h^*\|_{L^2}^2 \leq C_2 h^\nu, \quad \text{for some } y_h^* \in Y_h^*.$$

2. *Suppose we run Algorithm 2M with arbitrary tolerances  $\{\varepsilon_i\}_{i=1}^{l-1}$  on the lowest  $l-1$  levels. There exists a threshold  $\tilde{\varepsilon}_l$  depending on  $\{\varepsilon_i\}_{i=1}^{l-1}$ , as long as we set  $\varepsilon_l \leq \tilde{\varepsilon}_l(\{\varepsilon_i\}_{i=1}^{l-1})$  on level  $l$ , we have*

$$(4.20) \quad \|y_{h_l}^{K_l} - y_{h_l}^*\|_{L^2}^2 \leq C_2 (h_l)^\nu, \quad \text{for some } y_{h_l}^* \in Y_{h_l}^*.$$

*Proof.* Define

$$\tilde{M} = \begin{bmatrix} I/\mu & I \\ I & I/\tau \end{bmatrix}.$$

Similar to Algorithm 1, Algorithm 2 is equivalent to PPA with the  $\tilde{M}$ -metric. Then we follow the same proof as that of Lemma 4.1 and obtain Lemma 4.4.  $\square$

Define the set of good stopping tolerances for Algorithms 2 and 2M:

$$(4.21) \quad \mathcal{T}_2 = \left\{ \varepsilon \mid \varepsilon \leq \tilde{\varepsilon} \right\},$$

$$(4.22) \quad \mathcal{T}_{2M} = \left\{ \{\varepsilon_l\}_{l=1}^L \mid \varepsilon_1 \leq \tilde{\varepsilon}_1, \varepsilon_2 \leq \tilde{\varepsilon}_2(\varepsilon_1), \dots, \varepsilon_L \leq \tilde{\varepsilon}_L(\{\varepsilon_l\}_{l=1}^{L-1}) \right\}.$$

THEOREM 4.5. *Given  $\rho^0, \rho^1, h, L \geq 2$  and  $h_l = 2^{L-l}h$  and Assumptions 3,4, if we take 0 as the initialization, then the following holds:*

1. *With  $\varepsilon \in \mathcal{T}_2$ , Algorithm 2 takes  $O(\frac{1}{\varepsilon})$  iterations to stop.*
2. *With  $\{\varepsilon_l\}_{l=1}^L \in \mathcal{T}_{2M}$ , Algorithm 2M takes  $O(\frac{1}{\varepsilon_l} h_l^\nu)$  iterations on level  $l$  ( $l \geq 2$ ).*

*Proof.* Firstly, we follow the same argument of step 1 in the proof of Theorem 4.2. Substituting  $-A_h$  with  $I$  and  $M_h$  with  $\tilde{M}$ , we obtain the following inequality similar to (4.14):

$$G_h^k \leq \frac{1}{k} \|y_h^0 - y_h^*\|_{\tilde{M}}^2 \leq \frac{3}{k} \|y_h^0 - y_h^*\|_{L^2}^2 = \frac{3}{k} \|y_h^*\|_{L^2}^2 \leq \frac{3C_3}{k}.$$

As long as  $k \geq \frac{3C_3}{\varepsilon}$ , the stopping condition  $G_h^k \leq \varepsilon$  is satisfied. Algorithm 2 takes  $K \leq \frac{3C_3}{\varepsilon} = O(1/\varepsilon)$  iterations to stop.

Similar to Algorithm 2, Algorithm 2M takes  $O(\frac{1}{\varepsilon_l})$  iterations for level  $l = 1$ . For level  $l \geq 2$ , we follow the same argument of step 2 in the proof of Theorem 4.2 and obtain

$$G_{h_l}^k \leq \frac{3}{k} \|y_{h_l}^0 - y_{h_l}^*\|_{L^2}^2 \leq \frac{3}{k} 4C_4(2h_l)^\nu = 12 \cdot 2^r C_4(h_l)^\nu \frac{1}{k}.$$

As long as  $k \geq 12 \cdot 2^r C_4(h_l)^\nu \frac{1}{\varepsilon_l}$ , the stopping condition  $G_{h_l}^k \leq \varepsilon$  is satisfied. Algorithm 2M takes  $K_l \leq 12 \cdot 2^r C_4(h_l)^\nu \frac{1}{\varepsilon_l} = O(\frac{1}{\varepsilon_l} h_l^\nu)$  iterations to stop.  $\square$

For Algorithm 2M, we choose the same stopping tolerance rule with that of Algorithm 1M (4.16) and obtain the following complexity analysis.

**THEOREM 4.6.** *Given  $\rho^0, \rho^1, h, h_l = 2^{L-l}h$  and Assumptions 3,4, if we take 0 as the initialization, the following holds:*

1. *With  $\varepsilon \in \mathcal{T}_2$ , the complexity of Algorithm 2 is*

$$(4.23) \quad \mathcal{O}_2 = O\left(\frac{1}{\varepsilon} \frac{d}{h^d} \log\left(\frac{1}{h}\right)\right).$$

2. *With  $\{\varepsilon_l\}_{l=1}^L$  taken by (4.16) and  $\{\varepsilon_l\}_{l=1}^L \in \mathcal{T}_{2M}$  and  $L = 1 + \log_2(1/h)$ , the complexity of Algorithm 2M is*

$$(4.24) \quad \mathcal{O}_{2M} = \begin{cases} O\left(\frac{1}{\varepsilon_L} \frac{d}{h^{d-\nu}} \log\left(\frac{1}{h}\right)\right) + O\left(\frac{d2^d}{h^d}\right), & \text{if } \alpha > \nu - d, \\ O\left(\frac{1}{\varepsilon_L} \frac{d}{h^{d-\nu}} \log^2\left(\frac{1}{h}\right)\right) + O\left(\frac{d2^d}{h^d}\right), & \text{if } \alpha = \nu - d, \\ O\left(\frac{1}{\varepsilon_L} \frac{d}{h^{-\alpha}} \log\left(\frac{1}{h}\right)\right) + O\left(\frac{d2^d}{h^d}\right), & \text{if } \alpha < \nu - d. \end{cases}$$

*Proof.* In each step of Algorithm 2, the dominant calculation is conducting a  $d$  dimensional FFT on  $\tilde{\varphi}_h^k$  [33], which have complexity of  $O(N^d \log(N^d))$ . Since  $N = 1/h$ , the complexity is  $O(\frac{d}{h^d} \log(\frac{1}{h}))$  [22]. Then the complexity of Algorithm 2 is:

$$\mathcal{O}_2 = O\left(\frac{1}{\varepsilon}\right) \times O\left(\frac{d}{h^d} \log\left(\frac{1}{h}\right)\right) = O\left(\frac{1}{\varepsilon} \frac{d}{h^d} \log\left(\frac{1}{h}\right)\right).$$

Thus, the complexity of Algorithm 2M on level  $l = 1$  is  $O(\frac{1}{\varepsilon_1} \frac{d}{h_1^d} \log(\frac{1}{h_1}))$ , and, on higher levels ( $2 \leq l \leq L$ ), is  $O(\frac{1}{\varepsilon_l} \frac{d}{h_l^{d-\nu}} \log(\frac{1}{h_l}))$ . Therefore, we have

$$\begin{aligned} \mathcal{O}_{2M,1} &= \sum_{l=2}^L O\left(\frac{1}{\varepsilon_l} \frac{d}{h_l^{d-\nu}} \log\left(\frac{1}{h_l}\right)\right) + O\left(\frac{1}{\varepsilon_1} \frac{d}{h_1^d} \log\left(\frac{1}{h_1}\right)\right) \\ &= \sum_{l=2}^L O\left(\frac{h^\alpha}{\varepsilon_L} \frac{d}{h_l^{d+\alpha-\nu}} \log\left(\frac{1}{h_l}\right)\right) + O\left(\frac{h^\alpha}{\varepsilon_L} \frac{d}{h_1^{d+\alpha}} \log\left(\frac{1}{h_1}\right)\right) \\ &= O\left(\frac{1}{\varepsilon_L} \frac{d}{h^{d-\nu}} \log\left(\frac{1}{h}\right)\right) \left(\sum_{i=0}^{L-2} 2^{-i(d+\alpha-\nu)} + 2^{-(d+\alpha)(L-1)} h^{-\nu}\right) \\ &= O\left(\frac{1}{\varepsilon_L} \frac{d}{h^{d-\nu}} \log\left(\frac{1}{h}\right)\right) \left(\sum_{i=0}^{L-1} 2^{-i(d+\alpha-\nu)}\right). \end{aligned}$$

Then following the same proof as that for Theorem 4.3, we obtain (4.24).  $\square$

**4.4. Summary of complexities.** Tables 1 and 2 summarize the complexities. Let  $N = 1/h$ , Table 1 can be directly derived from Theorems 4.3 and 4.6. In the case of  $d = 2$  (2D case), we choose typical parameters (tolerances in Section 3.4,  $r = 2, \nu = 1$ ) and compare Algorithms 1, 2, 1M and 2M with other EMD algorithms [35, 4] in Table 2. By [35], their algorithm has complexity of  $O((N^d)^2)$ . As  $d = 2$ , it is  $O(N^4)$ . The algorithm in [4] constructs a graph and solves the uncapacitated minimum cost flow problem on the graph. The worst case complexity is  $O(|V| \log(|V|)(|V| \log(|V|) + |E|))$ , where  $|V|$  is the number of nodes in the created graph and  $|E|$  is the number of edges. As  $p = 1$  or  $p = \infty$ ,  $|V| = O(N^2)$ ,  $|E| = O(N^2)$ , the complexity is  $O(N^4 \log^2(N))$ ; as  $p = 2$ ,  $|V| = O(N^2)$ ,  $|E| = O(N^4)$ , the complexity is  $O(N^6 \log(N))$ .

TABLE 1

Complexities of Algorithms 1, 2, 1M and 2M. The parameters  $r, \nu$  depend on the interpolation accuracy (Assumptions 2, 4). We take  $\varepsilon_l$  as (4.16) and  $\alpha \geq r - d - 1$  for Alg. 1M,  $\alpha \geq \nu - d$  for Alg. 2M.

$p = 1, 2, \infty$	
Algorithm 1 [34]	$O(d^{3/2} N^{d+1} \log(N)/\varepsilon)$
Algorithm 2 [33]	$O(dN^d \log^2(N)/\varepsilon)$
Algorithm 1M	$O(d^{3/2} N^{d+1-r} \log(N)/\varepsilon_L) + O(d2^d N^d)$
Algorithm 2M	$O(dN^{d-\nu} \log^2(N)/\varepsilon_L) + O(d2^d N^d)$

TABLE 2

Complexities in the 2D case ( $d = 2$ ). Algorithms 1, 2, 1M, 2M choose tolerances described in Section 3.4.

	$p = 1$	$p = 2$	$p = \infty$
Tree-EMD [35]	$O(N^4)$	-	-
Min-cost flow[4] <sup>5</sup>	$O(N^4 \log^2(N))$	$O(N^6 \log(N))$	$O(N^4 \log^2(N))$
Algorithm 1 [34]	$O(N^6)$	$O(N^6)$	$O(N^6)$
Algorithm 2 [33]	$O(N^4 \log(N))$	$O(N^4 \log(N))$	$O(N^4 \log(N))$
Algorithm 1M	$O(N^3 \log(N))$	$O(N^3 \log(N))$	$O(N^3 \log(N))$
Algorithm 2M	$O(N^3 \log^2(N))$	$O(N^3 \log^2(N))$	$O(N^3 \log^2(N))$

**5. Numerical validation of the assumptions.** We numerically validated Assumptions 1, 2, 3 and 4 in the case of dimension  $d = 2$  and  $p \in \{1, 2, \infty\}$ .

**5.1. Quantitative validation.** Table 3 reports our results. Since the EMD generally does not have a closed-form solution in the 2D case, we numerically estimate  $z_{h_l}^*, y_{h_l}^*$  ( $1 \leq l \leq L$ ) to validate the assumptions. By Theorem 1 in [34],  $z_{h_l}^k \rightarrow z_{h_l}^*$  as  $k \rightarrow \infty$  for all  $l$ . Consequently, as long as the stopping tolerance  $\varepsilon$  is small enough, we could use  $z_{h_l}^K$  obtained by Algorithm 1M to estimate  $z_{h_l}^*$ . In this section, we set  $\varepsilon = 10^{-8}$ . The same can be done to estimate  $y_{h_l}^*$ . We estimated  $z_{h_l}^*, y_{h_l}^*$  ( $1 \leq l \leq L$ ) on the instances in the DOTmark dataset [51] and calculated averages over the instances of the four values:  $\|z_{h_l}^*\|_{L^2}^2$ ,  $\|y_{h_l}^*\|_{L^2}^2$ ,  $\|\text{Interpolate}(z_{h_{l-1}}^*) - z_{h_l}^*\|_{L^2}^2$ ,  $\|\text{Interpolate}(y_{h_{l-1}}^*) - y_{h_l}^*\|_{L^2}^2$ .

<sup>5</sup>The complexity of solving the minimum cost flow problem is the upper bound for the worst case. In practice, their algorithm has better performance than the theoretical bound. Numerical results are reported in Table 8.

TABLE 3  
Validation of the assumptions

	$l = 1$ $h_l = 1/32$	$l = 2$ $h_l = 1/64$	$l = 3$ $h_l = 1/128$	$l = 4$ $h_l = 1/256$	$l = 5$ $h_l = 1/512$
Assumption 1: $\ z_{h_l}^*\ _{L^2}^2$					
$p = 1$	0.101	0.094	0.091	0.089	0.089
$p = 2$	0.061	0.057	0.056	0.055	0.055
$p = \infty$	0.056	0.053	0.052	0.051	0.051
Assumption 2: $\ \text{Interpolate}(z_{h_{l-1}}^*) - z_{h_l}^*\ _{L^2}^2$					
$p = 1$	$1.35 \times 10^{-3}$	$4.15 \times 10^{-4}$	$1.08 \times 10^{-4}$	$2.57 \times 10^{-5}$	$3.59 \times 10^{-6}$
$p = 2$	$5.34 \times 10^{-4}$	$1.71 \times 10^{-4}$	$4.40 \times 10^{-5}$	$9.67 \times 10^{-6}$	$1.97 \times 10^{-6}$
$p = \infty$	$8.79 \times 10^{-4}$	$2.93 \times 10^{-4}$	$7.08 \times 10^{-5}$	$2.07 \times 10^{-5}$	$6.77 \times 10^{-6}$
Assumption 3: $\ y_{h_l}^*\ _{L^2}^2$					
$p = 1$	2.019	1.984	1.972	1.967	1.965
$p = 2$	1.015	1.003	0.997	0.995	0.993
$p = \infty$	0.965	0.960	0.963	0.967	0.972
Assumption 4: $\ \text{Interpolate}(y_{h_{l-1}}^*) - y_{h_l}^*\ _{L^2}^2$					
$p = 1$	$2.55 \times 10^{-1}$	$1.33 \times 10^{-1}$	$4.42 \times 10^{-2}$	$1.01 \times 10^{-2}$	$3.30 \times 10^{-3}$
$p = 2$	$6.05 \times 10^{-2}$	$2.89 \times 10^{-2}$	$1.31 \times 10^{-2}$	$4.68 \times 10^{-3}$	$1.14 \times 10^{-3}$
$p = \infty$	$8.18 \times 10^{-2}$	$4.72 \times 10^{-2}$	$2.12 \times 10^{-2}$	$8.84 \times 10^{-3}$	$3.48 \times 10^{-3}$

Table 3 shows that  $\|z_{h_l}^*\|_{L^2}^2$  and  $\|y_{h_l}^*\|_{L^2}^2$  are both bounded by a constant independent of grid step size  $h_l$ . Furthermore,  $\|\text{Interpolate}(z_{h_{l-1}}^*) - z_{h_l}^*\|_{L^2}^2 \approx O((h_l)^2)$  and  $\|\text{Interpolate}(y_{h_{l-1}}^*) - y_{h_l}^*\|_{L^2}^2 \approx O(h_l)$ . The above conclusions directly validate Assumptions 1, 2, 3, 4 and  $r \approx 2, \nu \approx 1$ .

## 5.2. Visualization of the non-uniqueness cases.

*Visualization of  $z_{h_l}^*$ .* The solution set  $Z_{h_l}^*$  may have multiple solutions on each level. This phenomena is also studied in [34] with only one level. What we want to show in this paragraph is that, for each coarse level solution  $z_{h_l}^* \in Z_{h_l}^*$ , there is a finer level solution  $z_{h_{l+1}}^* \in Z_{h_{l+1}}^*$  that is close to  $z_{h_l}^*$ . Here we set  $p = 1$ . Figures 3 and 4 illustrate this point. First, we consider the primal solution  $m_{h_l}^*$ . With different initializations, we obtain two different optimal  $m_{h_l}^*$ s on level  $l = 1$ : Figures 3(a) and 3(d). With the results in Figures 3(a) and 3(d) as initializations, we obtain the solutions  $m_{h_l}^*$  on level 2: Figures 3(b) and 3(e). The flux in Figure 3(b) is close to that in Figure 3(a); Figure 3(e) is close to Figure 3(d). Thus, Assumption 2 is meaningful when there are multiple solutions on each level: for a solution  $m_{h_l}^*$  on level  $l$ , there is a solution  $m_{h_{l+1}}^*$  on level  $l + 1$  similar to  $m_{h_l}^*$ . Secondly, we consider the dual solution  $\phi_{h_l}^*$ . As  $p = 1$ ,  $\phi_{h_l}^*$  is unique up to a constant for each level  $l$ . The  $\phi_{h_l}^*$  on level  $l$  is close to that on the finer level  $\phi_{h_{l+1}}^*$ . Figure 4 demonstrates this point.

*Visualization of  $y_{h_l}^*$ .* We visualize  $y_{h_l}^*$  in a similar way. We set  $p = 1$  and get the results in Figures 5 and 6. Figure 5 shows that for a solution  $m_{h_l}^*$  on level  $l$ , there is a solution  $m_{h_{l+1}}^*$  on level  $l + 1$ , which is similar to  $m_{h_l}^*$ . On this specific numerical example, the dual variable  $\varphi_{h_l}^*$  is unique for each level  $l$ . Figure 6 demonstrates that  $\varphi_{h_l}^*$  on level  $l$  is close to  $\varphi_{h_{l+1}}^*$  on level  $l + 1$ .

**6. Numerical results.** In this section, we numerically study why and how much our Algorithms 1M and 2M speed up Algorithms 1 and 2. The conclusions in The-

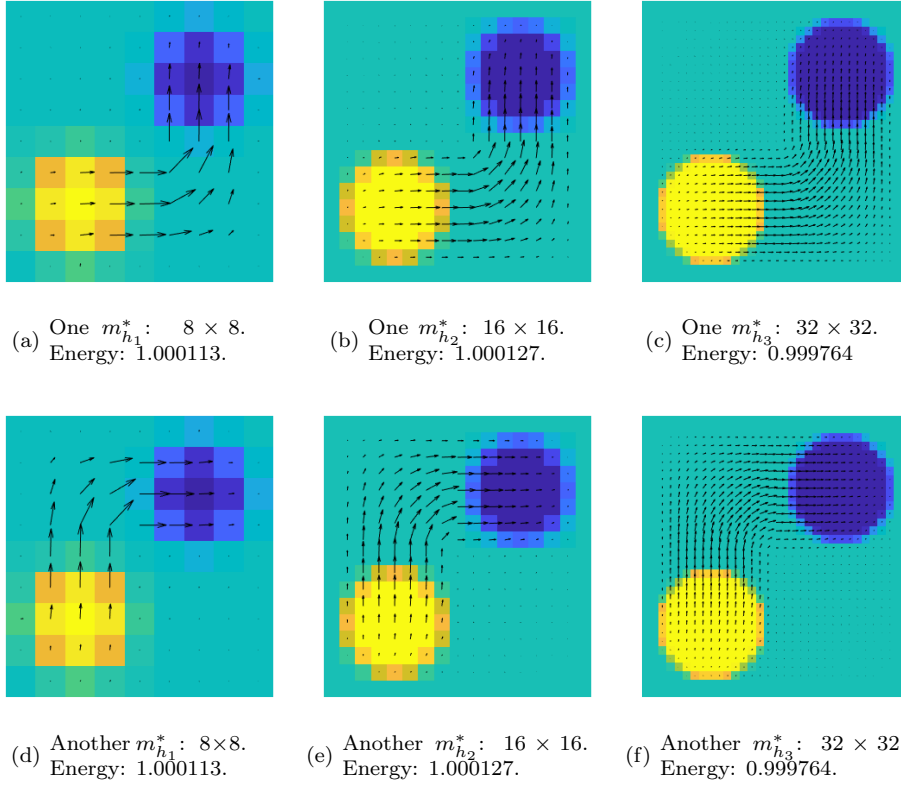


FIGURE 3. Visualization of Assumption 2: the black flux represents  $m_{h_l} : \Omega^{h_l} \rightarrow \mathbb{R}^2$ , the two circles represent  $\rho_{h_l}^0, \rho_{h_l}^1$  respectively. There are multiple solutions on each level. For every solution  $m_{h_l}^*$  on level  $l$ , there is a solution  $m_{h_{l+1}}^*$  on the finer level  $l+1$  that is similar to  $m_{h_l}^*$ .

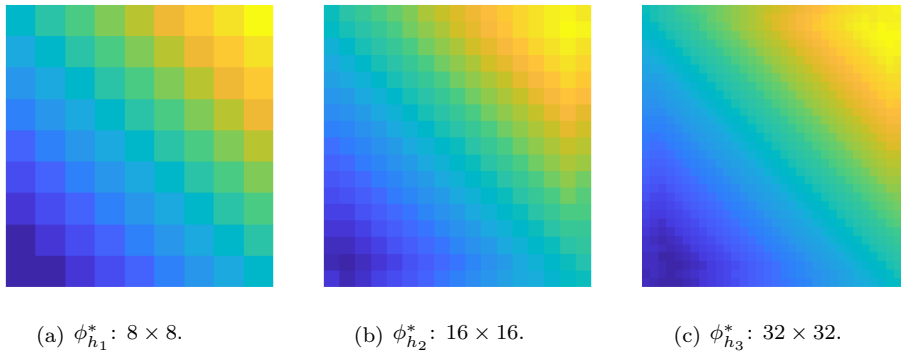


FIGURE 4. Visualization of Assumption 2: dual solution (Kantorovich potential)  $\phi_{h_l}^* : \Omega^{h_l} \rightarrow \mathbb{R}$  on each level. The dual solution  $\phi_{h_{l+1}}^*$  on level  $l+1$  is close to  $\phi_{h_l}^*$  on the coarser level  $l$ .

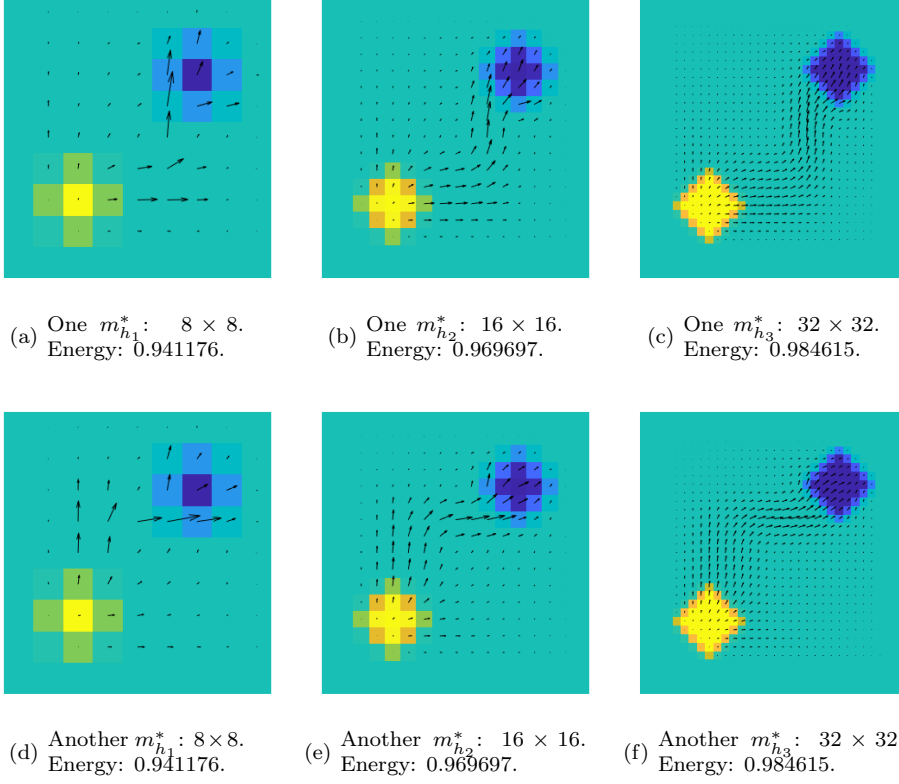


FIGURE 5. Visualization of Assumption 4: the black flux represents  $m_{h_l} : \Omega^{h_l} \rightarrow \mathbb{R}^2$ , the two circles represent  $\rho_{h_l}^0, \rho_{h_l}^1$  respectively. There are multiple solutions on each level. For every solution  $m_{h_l}^*$  on level  $l$ , there is a solution  $m_{h_{l+1}}^*$  on level  $l+1$  that is close to  $m_{h_l}^*$ .

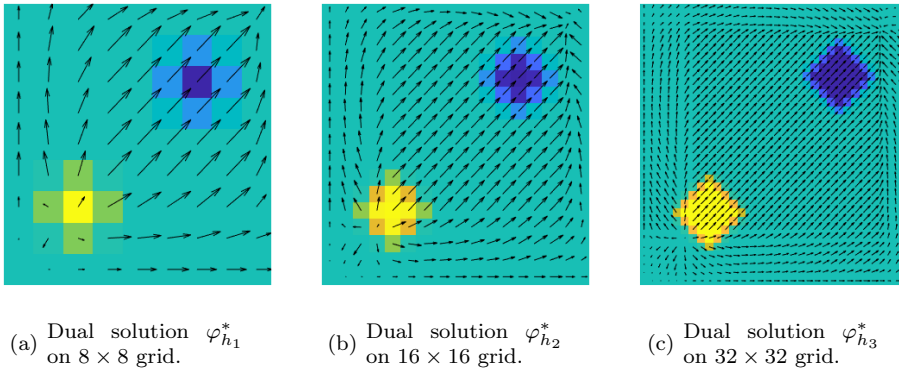


FIGURE 6. Visualization of Assumption 4: dual solution  $\varphi_{h_l}^* : \Omega^{h_l} \rightarrow \mathbb{R}^2$  on each level. The dual solution  $\varphi_{h_{l+1}}^*$  on level  $l$  is close to  $\varphi_{h_l}^*$  on level  $l+1$ .

orems 4.3 and 4.6 are validated. Moreover, we compare our algorithms with other EMD solvers [35, 4, 34, 33]. We implemented Algorithms 1M and 2M for  $d = 2$  in MATLAB. All the experiments were conducted on a single CPU (Intel i7-2600 CPU @ 3.40GHz).

**6.1. The effect of multilevel initialization.** In this subsection, we study why multilevel initialization helps speed up Algorithms 1 and 2. All the results are obtained on the “cat” example, which is also used as a benchmark in [34, 33], and  $p = 1$ . For Algorithm 1M, we choose  $\varepsilon_l = 10^{-6}$  for all levels. For Algorithm 2M, we choose  $\varepsilon_l = 10^{-5}$  for all levels. We report the results in Table 4.

TABLE 4

The effect of level number  $L$ . “Iters” is the number of iterations, and “Time” is in second.

Number of levels	Calculation cost on each level								Total time
	64 × 64		128 × 128		256 × 256		512 × 512		
	Iters	Time	Iters	Time	Iters	Time	Iters	Time	
Algorithm 1M									
L=1							5264	95.48	95.48
L=2					3036	10.76	30	0.550	11.31
L=3			1753	1.971	95	0.339	29	0.541	2.851
L=4	1002	0.456	242	0.291	105	0.395	31	0.572	1.714
Algorithm 2M									
L=1							100	2.375	2.375
L=2					99	1.224	2	0.113	1.337
L=3			99	0.157	4	0.095	2	0.121	0.373
L=4	100	0.024	8	0.019	4	0.097	2	0.121	0.261

*Algorithm 1M.* If  $L = 1$ , Algorithm 1M reduces to Algorithm 1, which takes 5264 iterations to stop as Table 4 shows. If  $L = 2$ , we first conduct 3036 iterations on a coarse grid  $256 \times 256$ . The obtained result is used to initialize the algorithm on the fine grid  $512 \times 512$ . With this initialization, Algorithm 1M only takes 30 iterations to stop on the fine grid. Although extra calculations on  $256 \times 256$  grid are required, the merit of fewer iterations on the fine grid overcomes the extra calculation cost. Thus, the total calculation time is reduced from 95.48 seconds to 11.31 seconds. When the number of levels  $L$  gets even larger, the computing time could be further reduced. The results support Theorem 4.2. Since the multilevel algorithm is able to dramatically reduce the calculation expense on the finest level, it consumes much less computing time.

*Algorithm 2M.* The advantage of Algorithm 2M is similar to that of Algorithm 1M. With  $L > 1$ , the number of iterations on the finest grid  $512 \times 512$  can be reduced from 100 to 2, and the calculation time is reduced from 2.375 seconds to 0.121 seconds.

**6.2. The effect of stopping tolerances.** In this subsection, we study tolerance rules for Algorithms 1M and 2M. With  $\alpha = 1, 0, -1, -5$ , formula (4.16) gives decreasing tolerance, constant tolerance and increasing tolerance respectively. For Algorithm 1M,  $\varepsilon_L$  is chosen from  $\varepsilon_L \in \{1 \times 10^{-6} \times 2^p : p \in \{0, -1, -2, \dots, -10\}\}$ . For Algorithm 2M,  $\varepsilon_L$  is chosen from  $\varepsilon_L \in \{1 \times 10^{-4} \times 2^p : p \in \{5, 4, 3, \dots, -10\}\}$ . We report the best  $\varepsilon_L$  and compare the three tolerance rules in Tables 5 and 6. The “best”  $\varepsilon_L$  takes the largest possible value that the algorithm meets the following condition:

$$(6.1) \quad |f(m_{h_l}^*) - f(m_{h_l}^{K_l})| < |f(m_{h_l}^*) - f(m_{h_{l-1}}^*)|, \quad l = 2, 3, \dots, L.$$

We use the above condition because (4.6) and (4.20) are intractable to numerically validate due to the non-uniqueness of  $z_{h_l}^*$  and  $y_{h_l}^*$ . We use the error in objective function value  $|f(m_{h_l}^*) - f(m_{h_l}^{K_l})|$  to estimate  $\|z_{h_l}^* - z_{h_l}^{K_l}\|^2$  and use the difference between the function values on two successive levels  $|f(m_{h_l}^*) - f(m_{h_{l-1}}^*)|$  to estimate the grid error. Once condition (6.1) is satisfied, we regard  $m_{h_l}^{K_l}$  close enough to  $m_{h_l}^*$ .

TABLE 5

Algorithm 1M on an example of size  $256 \times 256$ . “Error” means  $|f(m_{h_l}^*) - f(m_{h_l}^{K_l})|$ , “Time” is in seconds. Baseline: Algorithm 1 with  $\varepsilon = 1.6 \times 10^{-8}$ , 33232 iterations, time: 105.59 seconds.

Level	$l = 1$	$l = 2$	$l = 3$	$l = 4$	$l = 5$	$l = 6$
$h_l$	$h_l = 2^{-3}$	$h_l = 2^{-4}$	$h_l = 2^{-5}$	$h_l = 2^{-6}$	$h_l = 2^{-7}$	$h_l = 2^{-8}$
$ f(m_{h_l}^*) - f(m_{h_{l-1}}^*) $		1.1E-3	9.3e-4	5.8e-4	2.8e-4	1.3e-4
$\varepsilon_l = 1 \times 10^{-6}/512 \times (h_l/h_L)$						
$\varepsilon_l$	6.3E-8	3.1E-8	1.6E-8	7.8E-9	3.9E-9	2.0E-9
$K_l$	486	673	1526	3426	8401	12075
Time	0.055	0.065	0.204	1.121	8.494	39.22
Error	3.7E-4	2.8E-4	8.4E-5	2.6E-5	1.3E-4	6.4E-5
Total time: 49.17 secs. Speedup: $105.59/48.17 = 2.19$ .						
$\varepsilon_l = 1 \times 10^{-6}/128$						
$\varepsilon_l$	7.8E-9	7.8E-9	7.8E-9	7.8E-9	7.8E-9	7.8E-9
$K_l$	610	999	1921	3730	3806	4270
Time	0.063	0.092	0.254	1.617	3.483	13.46
Error	1.1E-4	1.9E-4	1.8E-4	6.8E-5	1.8E-4	1.4E-5
Total time: 18.98 secs. Speedup: $105.59/18.98 = 5.56$ .						
$\varepsilon_l = 1 \times 10^{-6}/32 \times (h_l/h_L)^{-1}$						
$\varepsilon_l$	9.8E-10	2.0E-9	3.9E-9	7.8E-9	1.6E-8	3.1E-8
$K_l$	735	1279	2351	4255	2459	932
Time	0.106	0.129	0.312	2.091	2.914	3.096
Error	2.3E-5	9.1E-5	6.5E-5	1.4E-4	2.4E-4	<b>2.3E-6</b>
Total time: 8.68 secs. Speedup: $105.59/8.68 = \mathbf{12.16}$ .						
$\varepsilon_l = 1 \times 10^{-6}/8 \times (h_l/h_L)^{-5}$						
$\varepsilon_l$	3.7E-15	1.2E-13	3.8E-12	1.2E-10	3.9E-9	1.3E-7
$K_l$	1483	3354	7716	16532	7286	<b>173</b>
Time	0.731	0.300	0.998	7.072	7.713	<b>0.614</b>
Error	9.7E-7	5.7E-7	2.4E-6	1.6E-5	2.3E-4	4.2E-6
Total time: 17.43 secs. Speedup: $105.59/17.43 = 6.06$ .						

Table 5 shows the significance of initialization for Algorithm 1M. With  $\alpha = 1$ , Algorithm 1M sets larger tolerance on the lower levels and the corresponding error is larger. Since we initialize level  $l = 6$  with the results on the lower levels ( $1 \leq l \leq 5$ ), such tolerance rule leads to inaccurate initialization and larger number of iterations on level  $l = 6$ . Calculations on the finest level are more computational complex than those on the coarser levels. Thus, the decreasing tolerance rule ( $\alpha = 1$ ) is not efficient. The increasing tolerances ( $\alpha = -1, -5$ ) fix this issue. They invest more computations on the lower levels and takes less computations on the finest level. Then the total computing time is dramatically reduced. However, if the  $\alpha$  is too small, say  $\alpha = -5$ , the algorithm costs more overheads on the lower levels that hurt the total computing

time, which validates Theorem 4.3. Thus,  $\alpha = -1$  is a good choice.

Table 6 demonstrates similar properties of Algorithm 2M. With a decreasing tolerance rule ( $\alpha = 1$ ), the algorithm takes 42 steps on level  $l = 6$ , while this number for the increasing tolerances ( $\alpha = -1, -5$ ) rule is only 1. And  $\alpha = -5$  over-invests calculations on lower levels and costs more time than  $\alpha = -1$ .

TABLE 6

Algorithm 2M on an example of  $512 \times 512$ . “Error” means  $|f(m_{h_l}^*) - f(m_{h_l}^{K_l})|$ , “Time” is in seconds, and the bold texts give the best results. Baseline: Algorithm 2 with  $\varepsilon = 6.25 \times 10^{-6}$ , 120 iterations, time consumption: 2.595 seconds.

Level	$l = 1$	$l = 2$	$l = 3$	$l = 4$	$l = 5$	$l = 6$
$h_l$	$h_l = 2^{-4}$	$h_l = 2^{-5}$	$h_l = 2^{-6}$	$h_l = 2^{-7}$	$h_l = 2^{-8}$	$h_l = 2^{-9}$
$ f(m_{h_l}^*) - f(m_{h_{l-1}}^*) $		2.0E-3	1.0E-3	5.3E-4	2.4E-4	9.6E-5
$\varepsilon_l = 1 \times 10^{-4}/16 \times (h_l/h_L)$						
$\varepsilon_l$	2.0E-4	1.0E-4	5.0E-5	2.5E-5	1.25E-5	6.25E-6
$K_l$	37	10	8	12	19	42
Time	0.001	0.001	0.003	0.020	0.249	0.955
Error	3.6E-4	5.5E-4	3.2E-4	3.0E-4	1.5E-4	8.9E-5
Total time: 1.287 secs. Speedup: $2.595/1.287 = 2.02$ .						
$\varepsilon_l = 1 \times 10^{-4}/32$						
$\varepsilon_l$	3.1E-6	3.1E-6	3.1E-6	3.1E-6	3.1E-6	3.1E-6
$K_l$	138	58	38	65	13	2
Time	0.002	0.003	0.009	0.089	0.181	0.113
Error	2.0E-5	4.5E-5	9.8E-5	7.4E-5	6.4E-5	6.2E-5
Total time: 0.458 secs. Speedup: $2.595/0.458 = 5.67$ .						
$\varepsilon_l = 1 \times 10^{-4}/32 \times (h_l/h_L)^{-1}$						
$\varepsilon_l$	9.8E-8	2.0E-7	3.9E-7	7.8E-7	1.6E-6	3.1E-6
$K_l$	352	547	22	69	2	<b>1</b>
Time	0.006	0.029	0.005	0.094	0.058	<b>0.068</b>
Error	1.5E-5	1.6E-5	4.6E-5	3.5E-5	5.3E-5	<b>5.8E-5</b>
Total time: 0.319 secs. Speedup: $2.595/0.319 = 8.13$ .						
$\varepsilon_l = 1 \times 10^{-4} \times 32 \times (h_l/h_L)^{-5}$						
$\varepsilon_l$	9.5E-11	3.1E-9	9.8E-8	3.1E-6	1.0E-4	3.2E-3
$K_l$	2433	1372	538	1	1	<b>1</b>
Time	0.037	0.075	0.113	0.005	0.037	<b>0.068</b>
Error	0	4.2E-17	5.5E-6	5.9E-5	7.4E-5	7.6E-5
Total time: 0.394 secs. Speedup: $2.595/0.394 = 6.59$ .						

**6.3. Comparison with other methods.** In this subsection, we compare our method with other EMD algorithms [35, 4, 34, 33]. There are some other 2D EMD solvers [42, 37, 52, 8, 19, 29] we do not compare with. [42] solves EMD with a thresholded metric; [37, 29] are designed for Wasserstein- $p$  ( $p > 1$ ) distance; [19, 52, 8] solve EMD with the entropy regularizer, the objective function of which is not the same as ours. Thus, we are not able to compare these algorithms with ours fairly in our settings.

All the results are obtained on the DOTmark [51] dataset. We used 10 images provided in the “classic images” of DOTmark. Totally we calculated 45 Wasserstein

TABLE 7

Errors of the algorithms with tolerance rule (6.2). “Cal. Err” means the calculation error:  $|f(m_h^*) - f(m_{h_L}^{KL})|$ . With (6.2), the calculation errors are comparable with the grid errors.

Grid size		$32 \times 32$	$64 \times 64$	$128 \times 128$	$256 \times 256$	$512 \times 512$
$p = 1$						
Grid Error $ f(m_{2h}^*) - f(m_h^*) $		1.15E-03	5.67E-04	2.82E-04	1.40E-04	
Cal. Err.	Alg. 1	2.02E-03	1.06E-03	4.80E-04	2.90E-04	N/A
	Alg. 1M	2.02E-03	1.06E-03	5.20E-04	3.08E-04	1.71E-04
	Alg. 2	1.21E-03	1.03E-03	6.82E-04	2.70E-04	1.05E-04
	Alg. 2M	1.10E-03	7.59E-04	4.43E-04	2.11E-04	9.62E-05
$p = 2$						
Grid Error $ f(m_{2h}^*) - f(m_h^*) $		9.68E-04	4.74E-04	2.34E-04	1.16E-04	
Cal. Err.	Alg. 1	1.83E-03	8.17E-04	4.63E-04	2.20E-04	N/A
	Alg. 1M	1.74E-03	9.45E-04	4.47E-04	2.59E-04	1.32E-04
	Alg. 2	8.95E-04	7.26E-04	4.74E-04	2.14E-04	9.83E-05
	Alg. 2M	1.26E-03	1.13E-03	5.84E-04	2.58E-04	1.11E-04
$p = \infty$						
Grid Error $ f(m_{2h}^*) - f(m_h^*) $		9.92E-04	5.14E-04	2.65E-04	1.36E-04	
Cal. Err.	Alg. 1	1.64E-03	1.02E-03	4.26E-04	2.23E-04	N/A
	Alg. 1M	1.60E-03	9.34E-04	4.65E-04	2.59E-04	1.09E-04
	Alg. 2	1.19E-03	9.16E-04	5.54E-04	2.51E-04	1.09E-04
	Alg. 2M	1.15E-03	9.82E-04	4.66E-04	2.57E-04	1.33E-04

distances for all the 45 image pairs. The time consumptions are averages taken on these image pairs. Figure 9 in Appendix D visualizes two such images and the optimal transport between them. Tree-EMD [35] and Min-cost flow [4] are exact algorithms stopping within finite steps. Other algorithms are iterative algorithms stopping by a tolerance. We take<sup>6</sup>  $L = \log_2(1/h) - 3$  and stopping tolerances as:

$$\begin{aligned}
 \varepsilon &= \frac{1 \times 10^{-6}}{512} \times \left(\frac{h}{1/512}\right)^3, & (\text{Alg. 1}) \\
 \varepsilon_l &= \varepsilon_L \times \left(\frac{h_l}{h}\right)^{-1}, \quad \varepsilon_L = \frac{1 \times 10^{-6}}{128} \times \left(\frac{h}{1/512}\right)^2, & (\text{Alg. 1M}) \\
 \varepsilon &= \min\left(2 \times 10^{-4}, \frac{1 \times 10^{-4}}{16} \times \left(\frac{h}{1/512}\right)^2\right), & (\text{Alg. 2}) \\
 \varepsilon_l &= \varepsilon_L \times \left(\frac{h_l}{h}\right)^{-1}, \quad \varepsilon = \min\left(2 \times 10^{-4}, \frac{1 \times 10^{-4}}{32} \times \left(\frac{h}{1/512}\right)^2\right). & (\text{Alg. 2M})
 \end{aligned}
 \tag{6.2}$$

These formulas are summarized from experiment results. With these stopping tolerances, one can usually obtain solutions accurate enough.

Table 7 reports the averaged errors on the examples of different sizes. The calculation errors is in the same order the grid approximation error:

$$|f(m_h^*) - f(m_{h_L}^{KL})| \leq 1.5|f(m_{2h}^*) - f(m_h^*)|.$$

<sup>6</sup>The level number  $L$  here is slightly smaller than the theoretical number  $L = \log_2(1/h) + 1$  but asymptotically the same.

Thus, formulas given in (6.2) are practically fair.

Table 8 reports the time consumptions of all the algorithms. “N/A” means the average calculation time is larger than half an hour. On large-scale examples, Algorithm 1M is much faster than Algorithm 1 and Algorithm 2M is much faster than Algorithm 2. In most of the cases, Algorithm 2M is the best and Algorithms 1M and 2 are also competitive. All the first-order methods (Algorithms 1, 2, 1M, 2M) are robust to the parameter  $p$  in the ground metric  $\|\cdot\|_p$ . Tree-EMD [35] only works for  $p = 1$ ; the algorithm in [4] works well when  $p = 1, \infty$  and the grid size is not very large. As  $p = 2$ , the algorithm in [4] requires large amount of memory and calculation time.

TABLE 8  
Averaged time consumption (seconds) on the DOTmark [51] dataset.

Grid size	$32 \times 32$	$64 \times 64$	$128 \times 128$	$256 \times 256$	$512 \times 512$
$p = 1$					
Tree-EMD [35]	0.006	0.127	2.433	121.2	N/A
Min-cost flow [4]	0.002	0.024	0.342	7.164	157.7
Algorithm 1 [34]	0.058	0.732	6.797	66.801	N/A
Algorithm 1M	0.047	0.219	1.321	7.555	49.054
Algorithm 2 [33]	0.002	0.008	0.066	0.980	3.102
Algorithm 2M	<b>0.001</b>	<b>0.003</b>	<b>0.010</b>	<b>0.060</b>	<b>0.227</b>
$p = 2$					
Tree-EMD [35]	N/A	N/A	N/A	N/A	N/A
Min-cost flow [4]	0.082	1.863	N/A	N/A	N/A
Algorithm 1 [34]	0.045	0.440	3.306	30.890	N/A
Algorithm 1M	0.040	0.170	1.137	5.663	45.333
Algorithm 2 [33]	<b>0.002</b>	0.008	0.061	0.809	2.471
Algorithm 2M	<b>0.002</b>	<b>0.004</b>	<b>0.018</b>	<b>0.163</b>	<b>0.826</b>
$p = \infty$					
Tree-EMD [35]	N/A	N/A	N/A	N/A	N/A
Min-cost flow [4]	<b>0.002</b>	0.025	0.300	5.380	118.1
Algorithm 1 [34]	0.126	1.152	9.221	92.016	N/A
Algorithm 1M	0.076	0.322	1.919	11.124	83.981
Algorithm 2 [33]	<b>0.002</b>	0.007	0.053	0.707	2.257
Algorithm 2M	<b>0.002</b>	<b>0.004</b>	<b>0.025</b>	<b>0.268</b>	<b>1.416</b>

**7. Conclusion.** In this paper, we have proposed two multilevel algorithms for the computation of the Wasserstein-1 metric. The algorithms leverage the  $L_1$  type primal-dual structure in the minimal flux formulation of optimal transport. The multilevel setting provides very good initializations for the minimization problems on the fine grids. So it can significantly reduce the number of iterations on the finest grid. This consideration allows us to compute the metric between two  $512 \times 512$  images in about one second on a single CPU. It is worth mentioning that the proposed algorithm also provides the Kantorovich potential and the optimal flux function between two densities. They are useful for the related Wasserstein variation problems [39].

In future work, we will apply the multilevel method to optimal transport related minimization in mean field games and machine learning.

### Appendix A. The proof of Lemma 3.1.

*Proof.* First, we consider the interpolation of potential  $\phi_{h_{l-1}}$ . With  $\phi_{h_l} = \text{Interpolate}(\phi_{h_{l-1}})$ , we have

$$\begin{aligned}
\|\phi_{h_l}\|_{L^2}^2 &= \sum_{x \in \Omega^{h_l}} \phi_{h_l}^2(x) (h_l)^d \\
&= \sum_{x \in \Omega^{h_l}} \left( \frac{1}{2^{|\bar{J}|}} \sum_{|y_{j_1} - x_{j_1}| \leq h_l} \cdots \sum_{|y_{j_{|\bar{J}}}| - x_{j_{|\bar{J}}}| \leq h_l} \phi_{h_{l-1}}(y_J, y_{j_1}, y_{j_2}, \dots, y_{j_{|\bar{J}}}) \right)^2 (h_l)^d \\
&\leq \sum_{x \in \Omega^{h_l}} \left( \frac{1}{2^{|\bar{J}|}} \sum_{|y_{j_1} - x_{j_1}| \leq h_l} \cdots \sum_{|y_{j_{|\bar{J}}}| - x_{j_{|\bar{J}}}| \leq h_l} \phi_{h_{l-1}}^2(y_J, y_{j_1}, y_{j_2}, \dots, y_{j_{|\bar{J}}}) \right) (h_l)^d \\
&= \sum_{y \in \Omega^{h_{l-1}}} c(y) \phi_{h_{l-1}}^2(y) (h_l)^d.
\end{aligned}$$

The inequality in the third line above follows from Jensen's Inequality [13], and  $c(y)$  is a constant which can be bounded in the following way.

$\phi_{h_{l-1}}(y)$  contributes to the nodes within a  $d$  dimensional hypercube  $H(y) = \{x \in \Omega : \max_j |x_j - y_j| \leq h_l\}$ . First, we consider  $y$  as an interior point in  $\Omega$ . There are  $2^d$  vertices in  $H(y)$ , for each vertex, the weight is  $1/(2^d)$ . There are  $2^{d-1}d$  edges in  $H(y)$ , each edge contains a single point  $x \in \Omega^{h_l}$ ,  $\phi_{h_{l-1}}(y)$  contributes to  $\phi_{h_l}(x)$  with weight  $1/(2^{d-1})$ . Generally speaking, there are  $2^{d-n} \binom{d}{n}$   $n$ -dimensional hypercubes on the boundary of  $H(y)$  [18], each  $m$ -dimensional hypercube contains a single point  $x \in \Omega^{h_l}$ ,  $\phi_{h_{l-1}}(y)$  contributes to  $\phi_{h_l}(x)$  with weight  $1/(2^{d-n})$ . Moreover, the center of  $H(y)$  is  $y$ , which is also in  $\Omega^{h_l}$ ,  $\phi_{h_{l-1}}(y)$  contributes to  $\phi_{h_l}(y)$  with weight 1. Thus, for interior point  $y$ , we have

$$\begin{aligned}
c(y) &= \frac{1}{2^d} \times 2^d + \frac{1}{2^{d-1}} \times d2^{d-1} + \cdots + \frac{1}{2^{d-1}} \times 2^{d-1} \binom{d}{n} + \cdots + 1 \times 1 \\
&= \sum_{n=0}^d \binom{d}{n} = (1+1)^d = 2^d.
\end{aligned}$$

For  $y$  on the boundary of  $\Omega$ , there are less points in  $H(y) \cap \Omega^{h_l}$ , and the weight for each node is the same as above, thus,  $c(y) < 2^d$ . In one word,  $c(y) \leq 2^d$  for all  $y \in \Omega^{h_{l-1}}$ . Then, we obtain

$$\begin{aligned}
\|\phi_{h_l}\|_{L^2}^2 &\leq \sum_{y \in \Omega^{h_{l-1}}} c(y) \phi_{h_{l-1}}^2(y) (h_l)^d \leq \sum_{y \in \Omega^{h_{l-1}}} \phi_{h_{l-1}}^2(y) (2h_l)^d \\
&= \sum_{y \in \Omega^{h_{l-1}}} \phi_{h_{l-1}}^2(y) (h_{l-1})^d = \|\phi_{h_{l-1}}\|_{L^2}^2.
\end{aligned}$$

With the same proof line, the interpolation of  $m_{h_{l-1}}$  and  $\varphi_{h_{l-1}}$  can also be proved. Inequalities (3.12) are proved.  $\square$

### Appendix B. Kantorovich potential.

The Kantorovich potential can be obtained directly from the dual solution of (3.1). Thus, Algorithm 1 directly gives the potential  $\phi_h^* : \Omega^h \rightarrow \mathfrak{R}$ . Algorithm 2 solves (3.5) and gives the gradient of  $\phi_h^*$ :  $\varphi_h^* : \Omega^h \rightarrow \mathfrak{R}^d$ . We obtain  $\phi_h^*$  given  $\varphi_h^*$  by solving

$$A_h A_h^* \phi_h = A_h \varphi_h^*.$$

The boundary condition is given by (2.4). Thus, the Laplacian operator  $A_h A_h^*$  is invertible, where the solution is unique up to a constant shift. And  $\phi_h^*$  is given by

$$(B.1) \quad \phi_h^* = (A_h A_h^*)^{-1} A_h \varphi_h^*.$$

The inverse Laplacian operator can be calculated efficiently by the FFT [33].

### Appendix C. Visualization of the cat example.

The cat example is used in Section 6.1. We visualize the two distributions  $\rho^0, \rho^1$  and the optimal transport between them in this section. Figure 7 visualizes the primal-dual pair  $(m^*, \phi^*)$  obtained by Algorithm 1M, Figure 8 visualizes the primal-dual pair  $(m^*, \varphi^*)$  obtained by Algorithm 2M.

### Appendix D. Visualization of DOTmark.

The DOTmark dataset is used in Section 6.3. We visualize two of the distributions  $\rho^0, \rho^1$  and the optimal transport between them in Figure 9.

## REFERENCES

- [1] M. ARJOVSKY, S. CHINTALA, AND L. BOTTOU, *Wasserstein generative adversarial networks*, in Proceedings of the 34th International Conference on Machine Learning (ICML), 2017.
- [2] S. BARTELS AND S. HERTZOG, *Error bounds for discretized optimal transport and its reliable efficient numerical solution*, arXiv preprint arXiv:1710.04888, (2017).
- [3] S. BARTELS AND P. SCHÖN, *Adaptive approximation of the monge–kantorovich problem via primal-dual gap estimates*, ESAIM: Mathematical Modelling and Numerical Analysis, 51 (2017), pp. 2237–2261.
- [4] F. BASSETTI, S. GUALANDI, AND M. VENERONI, *On the computation of kantorovich-wasserstein distances between 2d-histograms by uncapacitated minimum cost flows*, arXiv preprint arXiv:1804.00445, (2018).
- [5] M. BECKMANN, *A continuous model of transportation*, Econometrica: Journal of the Econometric Society, (1952), pp. 643–660.
- [6] J.-D. BENAMOU AND Y. BRENIER, *A computational fluid mechanics solution to the monge-kantorovich mass transfer problem*, Numerische Mathematik, 84 (2000), pp. 375–393.
- [7] J.-D. BENAMOU AND G. CARLIER, *Augmented Lagrangian Methods for Transport Optimization, Mean Field Games and Degenerate Elliptic Equations*, Journal of Optimization Theory and Applications, 167 (2015), pp. 1–26.
- [8] J.-D. BENAMOU, G. CARLIER, M. CUTURI, L. NENNA, AND G. PEYRÉ, *Iterative bregman projections for regularized transportation problems*, SIAM Journal on Scientific Computing, 37 (2015), pp. A1111–A1138.
- [9] J.-D. BENAMOU, G. CARLIER, AND R. HATCHI, *A numerical solution to monge’s problem with a finsler distance as cost*, ESAIM: Mathematical Modelling and Numerical Analysis, 52 (2018), pp. 2133–2148.
- [10] R. J. BERMAN, *The sinkhorn algorithm, parabolic optimal transport and geometric monge-amp\ere equations*, arXiv preprint arXiv:1712.03082, (2017).
- [11] R. J. BERMAN, *Convergence rates for discretized monge-amp\ere equations and quantitative stability of optimal transport*, arXiv preprint arXiv:1803.00785, (2018).
- [12] F. A. BORNEMANN AND P. DEUFLHARD, *The cascadic multigrid method for elliptic problems*, Numerische Mathematik, 75 (1996), pp. 135–152.
- [13] S. BOYD AND L. VANDENBERGHE, *Convex optimization*, Cambridge university press, 2004.
- [14] G. CARLIER, V. DUVAL, G. PEYRÉ, AND B. SCHMITZER, *Convergence of entropic schemes for optimal transport and gradient flows*, SIAM Journal on Mathematical Analysis, 49 (2017), pp. 1385–1418.
- [15] A. CHAMBOLLE AND T. POCK, *A first-order primal-dual algorithm for convex problems with applications to imaging*, Journal of mathematical imaging and vision, 40 (2011), pp. 120–145.
- [16] Y. CHEN, T. T. GEORGIU, AND M. PAVON, *On the relation between optimal transport and schrödinger bridges: A stochastic control viewpoint*, Journal of Optimization Theory and Applications, 169 (2016), pp. 671–691.
- [17] Y. CHEN, T. T. GEORGIU, AND M. PAVON, *Optimal transport over a linear dynamical system*, IEEE Transactions on Automatic Control, 62 (2017), pp. 2137–2152.

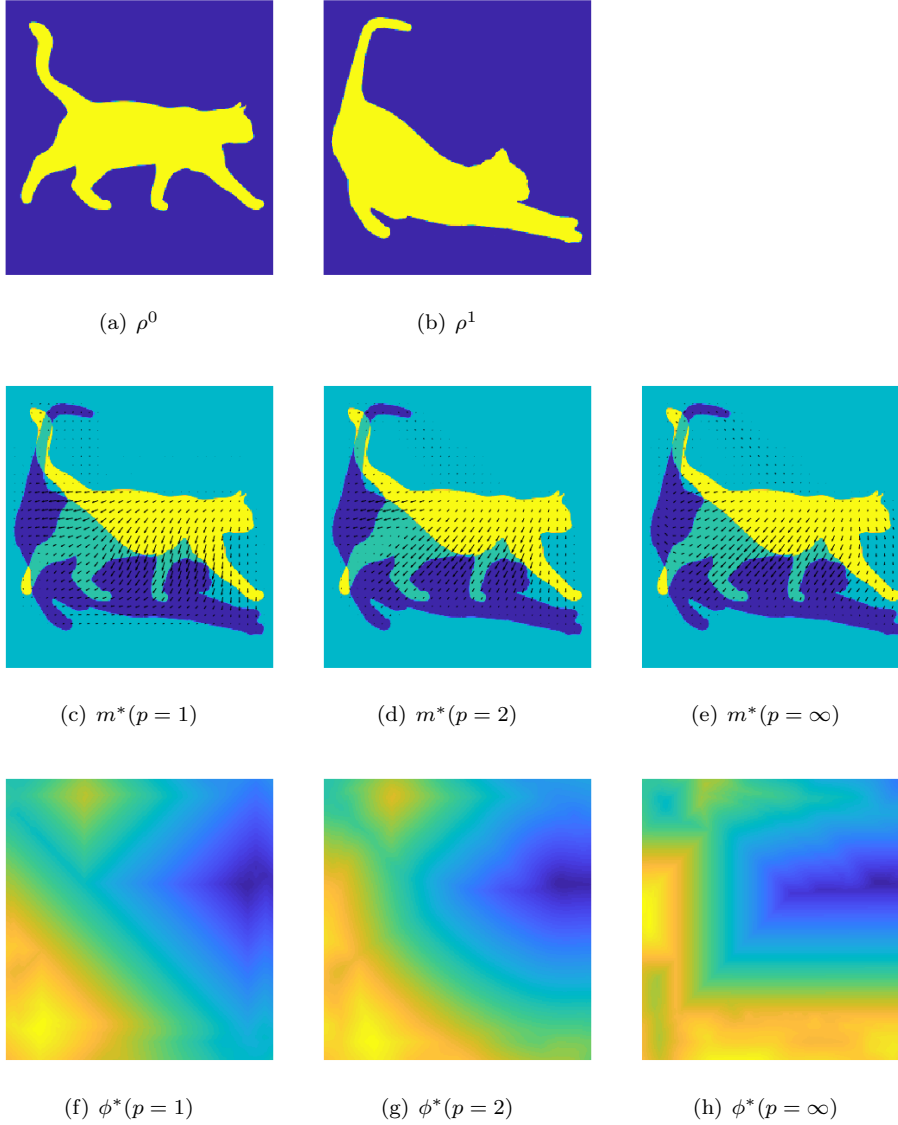


FIGURE 7. Visualization of  $(m^*, \phi^*)$  obtained by Algorithm 1M.  $m^*$  is the optimal flux;  $\phi^*$  is the Kantorovich potential. The backgrounds of Fig. 7(c), 7(d) and 7(e) are all  $\rho^0 - \rho^1$ .

- [18] H. S. M. COXETER, *Regular polytopes*, Courier Corporation, 1973.
- [19] M. CUTURI, *Sinkhorn distances: Lightspeed computation of optimal transport*, in Advances in neural information processing systems (NIPS), 2013, pp. 2292–2300.
- [20] M. CUTURI AND G. PEYRÉ, *A smoothed dual approach for variational wasserstein problems*, SIAM Journal on Imaging Sciences, 9 (2016), pp. 320–343.
- [21] J. DUCHI, S. SHALEV-SHWARTZ, Y. SINGER, AND T. CHANDRA, *Efficient projections onto the  $l_1$ -ball for learning in high dimensions*, in Proceedings of the 25th International Conference on Machine Learning (ICML), ACM, 2008, pp. 272–279.
- [22] P. DUHAMEL AND M. VETTERLI, *Fast fourier transforms: a tutorial review and a state of the art*, Signal processing, 19 (1990), pp. 259–299.
- [23] M. ESSID AND J. SOLOMON, *Quadratically regularized optimal transport on graphs*, SIAM

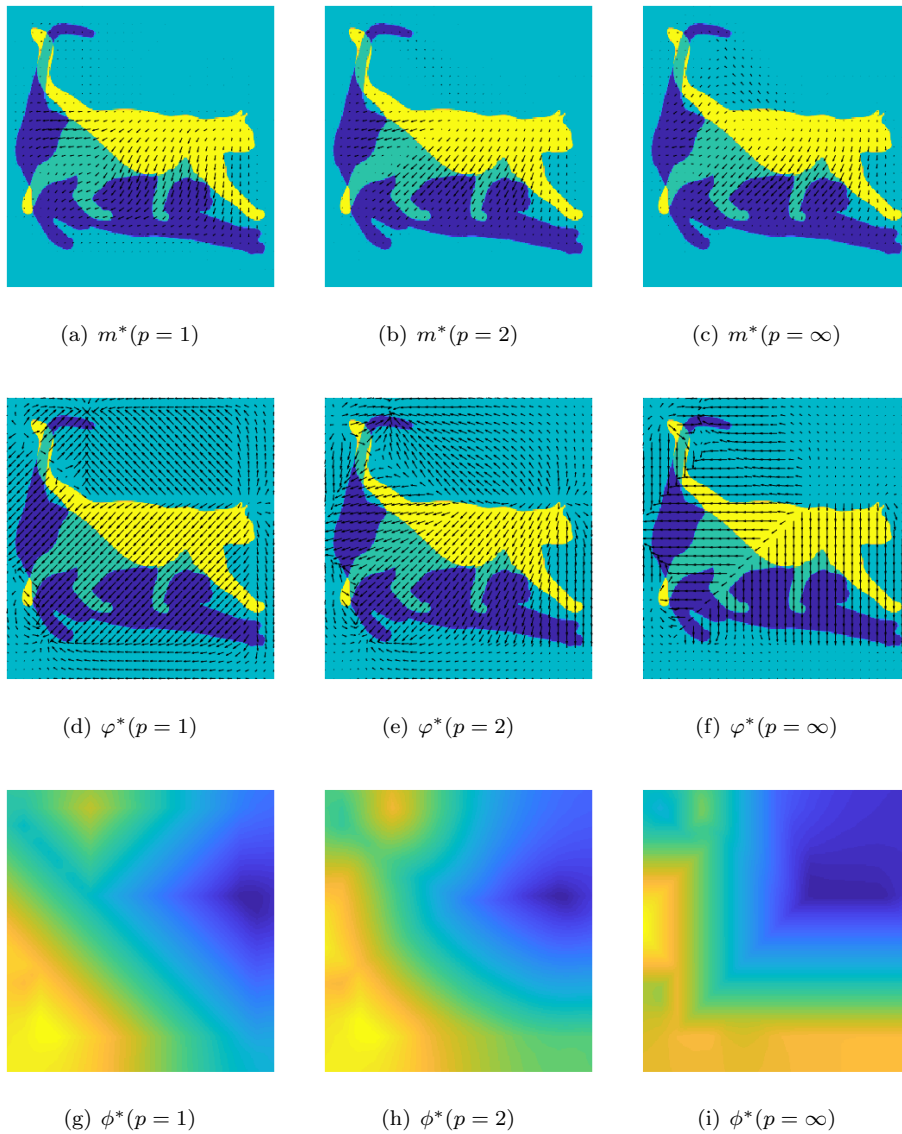
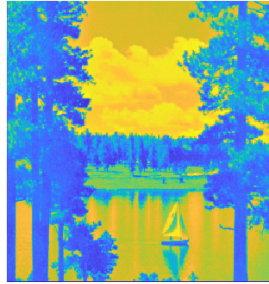


FIGURE 8. Visualization of  $(m^*, \varphi^*)$  and the potential  $\phi^*$  obtained by Algorithm 2M.  $\rho^0, \rho^1$  are the same with those in Figure 7.  $m^*$  is the optimal flux;  $\phi^*$  is the Kantorovich potential, that is obtained from  $\varphi^*$  by the method in Appendix B.

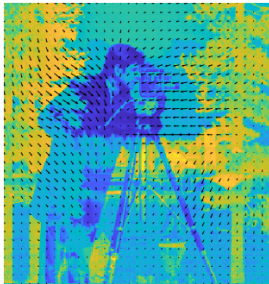
- Journal on Scientific Computing, 40 (2018), pp. A1961–A1986.
- [24] S. FERRADANS, N. PAPADAKIS, G. PEYRÉ, AND J.-F. AUJOL, *Regularized discrete optimal transport*, SIAM Journal on Imaging Sciences, 7 (2014), pp. 1853–1882.
- [25] C. FROGNER, C. ZHANG, H. MOBAHI, M. ARAYA, AND T. A. POGGIO, *Learning with a Wasserstein Loss*, in Advances in Neural Information Processing Systems 28, C. Cortes, N. D. Lawrence, D. D. Lee, M. Sugiyama, and R. Garnett, eds., Curran Associates, Inc., 2015, pp. 2053–2061.
- [26] W. GANGBO AND R. J. MCCANN, *The geometry of optimal transportation*, Acta Mathematica, 177 (1996), pp. 113–161.
- [27] G. H. GOLUB AND C. F. VAN LOAN, *Matrix computations*, vol. 3, JHU Press, 2012.



(a)  $\rho^0$ : Cameraman ( $512 \times 512$ ), one image of DOT-mark



(b)  $\rho^1$ : Lake ( $512 \times 512$ ), one image of DOTmark



(c)  $p = 1$



(d)  $p = 2$



(e)  $p = \infty$

FIGURE 9. Visualization of the optimal transport  $m^*$  between the two images  $\rho^0$  and  $\rho^1$ . The background is the difference between  $\rho^0, \rho^1$ :  $\rho = \rho^0 - \rho^1$ .

- [28] I. GULRAJANI, F. AHMED, M. ARJOVSKY, V. DUMOULIN, AND A. C. COURVILLE, *Improved training of wasserstein gans*, in Advances in Neural Information Processing Systems (NIPS), 2017, pp. 5767–5777.
- [29] E. HABER AND R. HORESH, *A multilevel method for the solution of time dependent optimal transport*, Numerical Mathematics: Theory, Methods and Applications, 8 (2015), p. 97–111, <https://doi.org/10.4208/nmtma.2015.w02si>.
- [30] V. HARTMANN AND D. SCHUHMACHER, *Semi-discrete optimal transport-the case  $p = 1$* , arXiv preprint arXiv:1706.07650, (2017).
- [31] B. HE AND X. YUAN, *Convergence analysis of primal-dual algorithms for a saddle-point problem: From contraction perspective*, SIAM J. Imaging Sciences, 5 (2012), pp. 119–149.
- [32] F. S. HILLIER AND G. J. LIEBERMAN, *Introduction to mathematical programming*, vol. 2, McGraw-Hill New York, 1995.
- [33] M. JACOBS, F. LÉGER, W. LI, AND S. OSHER, *Solving large-scale optimization problems with a convergence rate independent of grid size*, arXiv preprint arXiv:1805.09453, (2018).
- [34] W. LI, E. K. RYU, S. OSHER, W. YIN, AND W. GANGBO, *A parallel method for earth mover’s distance*, Journal of Scientific Computing, 75 (2018), pp. 182–197.
- [35] H. LING AND K. OKADA, *An Efficient Earth Mover’s Distance Algorithm for Robust Histogram Comparison*, IEEE Transactions on Pattern Analysis and Machine Intelligence, 29 (2007), pp. 840–853.
- [36] Q. MÉRIGOT, *A multiscale approach to optimal transport*, in Computer Graphics Forum, vol. 30, Wiley Online Library, 2011, pp. 1583–1592.
- [37] A. M. OBERMAN AND Y. RUAN, *An efficient linear programming method for optimal transportation*, arXiv preprint arXiv:1509.03668, (2015).
- [38] F. OTTO AND C. VILLANI, *Generalization of an inequality by talagrand and links with the*

- logarithmic sobolev inequality*, Journal of Functional Analysis, 173 (2000), pp. 361–400.
- [39] N. PAPADAKIS, G. PEYRÉ, AND E. OUDET, *Optimal Transport with Proximal Splitting*, SIAM Journal on Imaging Sciences, 7 (2014), pp. 212–238.
- [40] N. PARIKH, S. BOYD, ET AL., *Proximal algorithms*, Foundations and Trends® in Optimization, 1 (2014), pp. 127–239.
- [41] O. PELE AND M. WERMAN, *A linear time histogram metric for improved sift matching*, in Proceedings of the 10th European Conference on Computer Vision (ECCV), Springer, 2008, pp. 495–508.
- [42] O. PELE AND M. WERMAN, *Fast and robust Earth Mover’s Distances*, in 2009 IEEE 12th International Conference on Computer Vision (ICCV), 2009, pp. 460–467.
- [43] H. PETZKA, A. FISCHER, AND D. LUKOVNICOV, *On the regularization of wasserstein gans*, arXiv preprint arXiv:1709.08894, (2017).
- [44] G. PEYRÉ AND M. CUTURI, *Computational Optimal Transport*, arXiv:1803.00567 [stat], (2018), <https://arxiv.org/abs/1803.00567>.
- [45] Y. RUBNER, C. TOMASI, AND L. J. GUIBAS, *The earth mover’s distance as a metric for image retrieval*, International journal of computer vision, 40 (2000), pp. 99–121.
- [46] E. K. RYU, Y. CHEN, W. LI, AND S. OSHER, *Vector and Matrix Optimal Mass Transport: Theory, Algorithm, and Applications*, arXiv:1712.10279 [cs, math], (2017), <https://arxiv.org/abs/1712.10279>.
- [47] E. K. RYU, W. LI, P. YIN, AND S. OSHER, *Unbalanced and Partial  $L_1$  Monge-Kantorovich Problem: a Scalable Parallel First-Order Method*, Journal of Scientific Computing, 75 (2018), pp. 1596–1613.
- [48] B. SCHMITZER, *A sparse multiscale algorithm for dense optimal transport*, Journal of Mathematical Imaging and Vision, 56 (2016), pp. 238–259.
- [49] B. SCHMITZER AND B. WIRTH, *Dynamic models of wasserstein-1-type unbalanced transport*, arXiv preprint arXiv:1705.04535, (2017).
- [50] B. SCHMITZER AND B. WIRTH, *A framework for wasserstein-1-type metrics*, arXiv preprint arXiv:1701.01945, (2017).
- [51] J. SCHRIEBER, D. SCHUHMACHER, AND C. GOTTSCHLICH, *Dotmark—a benchmark for discrete optimal transport*, IEEE Access, 5 (2017), pp. 271–282.
- [52] J. SOLOMON, F. DE GOES, G. PEYRÉ, M. CUTURI, A. BUTSCHER, A. NGUYEN, T. DU, AND L. GUIBAS, *Convolutional wasserstein distances: Efficient optimal transportation on geometric domains*, ACM Transactions on Graphics (TOG), 34 (2015), p. 66.
- [53] J. SOLOMON, R. RUSTAMOV, L. GUIBAS, AND A. BUTSCHER, *Earth Mover’s Distances on Discrete Surfaces*, ACM Transactions on Graphics, Proceedings of ACM SIGGRAPH 2014, 33 (2014), pp. 1–12.
- [54] C. VILLANI, *Optimal transport: old and new*, vol. 338, Springer Science & Business Media, 2008.
- [55] P. WESSELING, *Introduction To Multigrid Methods*, R.T. Edwards, Inc., 2004.